



UNIVERSIDAD  
DE MÁLAGA



Máster Universitario  
en Simulación Numérica  
en Ciencia e Ingeniería  
con COMSOL Multiphysics

# MASTER THESIS

## COMSOL MODEL FOR THE CAPILLARY BREAKUP EXTENSIONAL ELECTORRHEOMETRY (CABEER) APPLIED TO FUNCTIONAL INKSAREA

MASTER DEGREE in

NUMERICAL SIMULATION IN SCIENCE AND  
ENGINEERING WITH COMSOL MULTIPHYSICS  
(2020/2021)

**AUTHOR:** FRANCISCO JOSÉ GALINDO ROSALES

**SUPERVISOR:** EMILIO RUIZ REINA

MÁLAGA, JUNIO DE 2021



---

# **COMSOL MODEL FOR THE CAPILLARY BREAKUP EXTENSIONAL ELECTORRHEOMETRY (CABEER) APPLIED TO FUNCTIONAL INKS AREA**

**Author:** Francisco José Galindo Rosales

**Supervisor:** Emilio Ruiz Reina

**Department:** Applied Physics II

**Degree:** Master Degree in Numerical Simulation in Science and Engineering with  
COMSOL MULTIPHYSICS

**Keywords:** Functional inks, CaBEER, numerical simulation.

## **Abstract**

Electrohydrodynamics jet (e-jet) printing process is an electrostatic-based ink-jet printing technique able to produce submicron dots, lines and patterns beyond the limited resolution of conventional ink-jet printing and for that reason, it can represent a paradigm shift for printed electronics manufacturing. Magnetic inks are very promising materials for different applications, such as security printing; however, its printability with traditional inkjet printing technique faces many technical difficulties and e-jet printing emerges as a potential alternative.

It is well known the importance of understanding the filament thinning process of inks that will be used in an inkjet printing process. For the same reason, it would be important to understand the filament thinning process under the simultaneous application of an external electric field aligned in the direction of the

---

flow, for those samples to be used in the e-jet printing processes. This is exactly the kind of experimental information that the Capillary Breakup Extensional Electrorheometry (CaBEER) device provides. Preliminary CaBEER experiments with a colloidal suspension of magnetite in a light hydrocarbon oil revealed that there is a critical electric field beyond which the filament thinning process changes from Newtonian-like to viscoelastic-like behaviour. It has been speculated that this change in the rheological behaviour can only be due to a change in the microstructure of the suspension, but the truth is that there are no scientific shreds of evidence supporting this hypothesis. Besides, if that statement was still correct, it would be needed to get better insight into the key parameters controlling this rearrangement in the internal microstructure.

This work contains the first attempt to develop a COMSOL model containing the physics behind the capillary thinning process of a functional ink, which consists of a colloidal suspension of magnetic nanoparticles in light hydrocarbon oil, under the presence of an external electric field aligned with the axis of the liquid filament. A complete model would allow for numerical analysis of the capillary breakup extensional electrorheometry (CaBEER) applied to functional inks.

To my children Helena and Diego,  
you are both a constant source  
of inspiration and motivation.

*F.J. Galindo-Rosales*



# Acknowledgements

I would like to express my gratitude to Prof. Emilio Ruiz Reina for his guidance, patience and support during the development of this dissertation.

I would also like to thank you Laura for being always very supportive and providing me with extra time at home to finish this master, particularly during the several pandemic lockdown periods that we have faced since the beginning of the course.

I would like to acknowledge the financial support through the R&D Project RheoOptimized2Dinks - PTDC/EME-APL/30765/2017 - POCI-01-0145-FEDER-030765 - funded by FEDER funds through COMPETE2020 - Programa Operacional Competitividade e Internacionalização (POCI) and with the financial support of FCT/MCTES through national funds (PIDDAC), and through the Principal Investigator Grant 2020.03203.CEECIND funded by FCT/MCTES through the Stimulus of Scientific Employment programme.

*F.J. Galindo-Rosales*





*“Learning is the only thing the  
mind never exhausts of, never  
fears to, and never regrets of”.*

---

Leonardo da Vinci (1452 - 1519)



# Preface

This Master Thesis is framed within the activities of the research project *RheoOptimized2Dinks* (*Rheologically optimized 2D-material-based inks*), which aims at providing a first step towards a fundamental understanding of the multiphysics problem of characterizing functional inks by means of capillary breakup extensional electrorheometry (CaBEER), and with the activities of the Principal Investigator Grant entitled *Electrohydrodynamics of ViscoElastic fluids* (*EHDViscoElastic*).

*F.J. Galindo-Rosales*



# Contents

<b>Abstract</b>	<b>iii</b>
<b>Acknowledgements</b>	<b>vii</b>
<b>Preface</b>	<b>xi</b>
1 Introduction. . . . .	7
1.1 Area of application . . . . .	8
1.2 State-of-the-art . . . . .	10
1.2.1 E-jet printing . . . . .	10
1.2.2 Magnetic inks . . . . .	13
1.2.3 Electrorheology . . . . .	14
1.3 Objective . . . . .	20
1.4 Methodology . . . . .	21
1.5 Document structure . . . . .	21

---

2	Capillary Breakup Extensional Electrorheometry . . . . .	23
2.1	Experimental setup . . . . .	24
2.2	Working fluids . . . . .	25
3	Modelling . . . . .	29
3.1	Introduction . . . . .	30
3.2	Model Definition . . . . .	32
3.3	Problem formulation . . . . .	33
3.3.1	Two-phase Flow, Phase field . . . . .	33
3.3.2	Electrostatic . . . . .	36
3.3.3	Particle Tracing for Fluid Flow . . . . .	38
3.3.4	Initial and boundary conditions . . . . .	43
4	Implementation, results and discussion. . . . .	45
4.1	Two-phase Flow . . . . .	46
4.2	Particle Tracing for Fluid Flow . . . . .	53
4.2.1	External forces . . . . .	55
4.2.2	Inter-particle force . . . . .	57
4.3	CaBEER model . . . . .	59
4.4	CaBEER-APP . . . . .	61
5	Final remarks and future works . . . . .	63
	Bibliografía . . . . .	71

# List of Figures

1.1	Comparison of the three EHD printing methods. Adapted from Ref. [1]. . . . .	11
1.2	Schematic illustration of the conventional ink-jet printing (a) and the e-jet printing (b).The liquid meniscus at the nozzle tip and the evolution of the shape of a Taylor cone during the e-jet printing (c). Reproduced with permission from Ref. [1]. . . . .	12
1.3	An embodiment of an electrorheological clutch proposed by W.M. Winslow in 1947: the power driving shaft (10) provided with a disc (11) translates its movement to a driven shaft (12) via another disc (13) closely spaced and insulated by means of an electrorheological fluid (14), held between them by capillary forces; the two shafts are connected to an electrical circuit (15-17). Image extracted from Ref. [2] via Google Patents. . . . .	14
1.4	ERF consisting of 1.5 $\mu\text{m}$ glass spheres suspended in silicone oil. Structural evolution of dielectric microspheres under an increasing electric field, from (a) no field, to (b) 500 V/mm, to (c) 900 V/mm. Reproduced from Ref. [3] with permission from The Royal Society of Chemistry. . . . .	16
1.5	Commercial rheometers equipped with electrorheological cells. Reproduced with permission from Ref. [4]. . . . .	17

1.6	Four different flow/electric fields configurations in electrorheometry. . . .	18
1.7	Three prototypical geometries for studying breakup of complex fluids; (a) continuous jetting instability; (b) dripping from a nozzle; (c) necking and breakup of a liquid bridge. [5] . . . . .	19
2.1	Schematic representation of the CaBEER experiment. . . . .	24
2.2	Time evolution of the minimum diameter of the ferrofluid EMG905 obtained in CaBEER experiments (reproduced with permission from [6]). .	27
3.1	Typical stability diagram of liquid bridges between equal disks subjected to a small constant axial acceleration [measured by Bond number: $Bo = 0.1$ (solid line), $Bo = 0$ (dashed line)]. Reprinted from [7], with the permission of AIP Publishing. . . . .	31
3.2	Fluid domain (left), where the liquid phase is highlighted in purple; and fluid interface (right), where the liquid sample is in red ( $V_f = 1$ ), the gas phase is in blue ( $V_f = 0$ ) and the interface is a band around $V_f = 0.5$ . . .	32
3.3	Schematic representation of the ink filament containing the colloidal particles undergone to the particle-particle force due to the induced dipoles and the three external forces (Brownian, drag and gravitational). . . . .	40
4.1	Printscreen showing the general view of the Two-Phase Flow model.	46
4.2	Definition of geometric parameters and surface tension, either as a constant parameter or as a variable if Marangoni effect were intended to be simulated. . . . .	47
4.3	The viscosity and density of the two fluids are defined as material properties: liquid in purple (left) and gas in grey (right). . . . .	48



---

4.4	Definition of the Laminar flow interface. . . . .	48
4.5	Definition of the Phase Field interface. . . . .	49
4.6	Definition of the Multiphysics <i>Two-Phase Flow, Phase Field</i> coupling. . . . .	50
4.7	Settings for two-step study used to solve the coupled problem. . . . .	51
4.8	Time evolution of the filament silhouette for the same fluid with the same conditions, except for the aspect ratio: $\Lambda_1 = 1.5$ for 1 ms and no breakup (top row) and $\Lambda_2 = 5$ for 0.14 ms (bottom row). . . . .	52
4.9	Last filament silhouette before breakup for the same fluid with the same conditions, except for the surface tension coefficient. In the case of the $\sigma = 0.02$ the filament was stable. . . . .	52
4.10	Printscreen showing the general view of the Particle Tracing model. . . . .	53
4.11	Definition of geometric parameters and particle properties required for the Particle Tracing model (left), as well as the properties of the liquid carrying the particles (right). . . . .	53
4.12	Settings for the Particle Tracing for Fluid Flow (top-left), particle properties (top-right) and the release of the particles (bottom). . . . .	54
4.13	Settings for the Particle Tracing for Fluid Flow (left), particle properties (middle) and the release of the particles (right). . . . .	56
4.14	Particle trajectories for different particle sizes after 1 ms after having been released: $r_p = \{100 \text{ nm}, 500 \text{ nm}, 1 \text{ }\mu\text{m}, 500 \text{ }\mu\text{m}\}$ (from left to right). . . . .	56
4.15	The electrostatic interface is added to the model. The liquid domain is set as a Ferroelectric material following the Langevin Function for its polarization. . . . .	57

---

4.16 Settings for the two-step study in the case of considering the inter-particle force due to polarization. . . . .	58
4.17 Error message when considering the contribution of the polarization forces. . . . .	58
4.18 Printscreen showing the general view of the CaBEER model. . . . .	59
4.19 Settings for the drag force applied to the particles when coupled with the fluid flow in the liquid sample (left). Settings for the third step in the study, where the Particle Tracing for fluid flow is solved with time after the fluid flow and the interface have been solved first.	60
4.20 Printscreen of the CaBEER-APP. . . . .	61

# Chapter 1

## Introduction

### Content

---

<b>1.1 Area of application</b> . . . . .	<b>8</b>
<b>1.2 State-of-the-art</b> . . . . .	<b>10</b>
1.2.1 E-jet printing . . . . .	10
1.2.2 Magnetic inks . . . . .	13
1.2.3 Electrorheology . . . . .	14
<b>1.3 Objective</b> . . . . .	<b>20</b>
<b>1.4 Methodology</b> . . . . .	<b>21</b>
<b>1.5 Document structure</b> . . . . .	<b>21</b>

---

## 1.1 Area of application

Printed electronics refers to the application of printing techniques to fabricate electronic structures, devices and circuits, processing a functional material (ink) from the liquid phase onto a substrate. The portfolio of fabrication techniques for printed electronics comprises a wide range of methods, including screen [8], gravure [9], flexographic [10], inkjet [11], aerosol jet printing [12], and electrohydrodynamic jet (e-jet) printing [13], which have been widely used for the fabrication of thin-film transistors, radiofrequency identifications, displays, etc.

The use of electrohydrodynamically induced fluid flows through fine micro-capillary nozzles allow producing ink droplets much smaller than the nozzle and because of that the e-jet printing has been regarded as a high-resolution printing technique, able to produce patterns and functional devices with submicrometre resolution, approaching 25 nm against the 1-2 microns for the competing piezo and thermal inkjet processes [14]. This electrostatic based ink-jet print system is a contactless printing process capable of printing submicron dots, lines and patterns with a wide range of functional “ink” materials including polymers, nanoparticle suspensions, and biomaterials, being the viscosity ( $1 - 1000 \text{ mPa} \cdot \text{s}$ ) and conductivity ( $10^{-6} - 10^{-1} \text{ S/m}$ ) the key parameters for the ink [15].

Magnetic inks are perspectives materials for security printing, coding and marking, magnetic device fabrication and creation of micro-antennas. The implementation of inkjet printing technique for magnetic applications seemed to be very promising; however, nowadays it is rather limited, mainly because a number of factors, including the difficulties in the synthesis of stable colloids of magnetic nanoparticles and adaptation of their rheological parameters [16]. Thus, e-jet printing emerges as a potential substituting printing technique for magnetic inks.

Extensional flows and the underlying stability/instability mechanisms are of extreme relevance to the efficient generation of micro droplets. Thus, the rheological characterization of magnetic inks, particularly under uniaxial extensional flow, is of paramount importance for e-jet printing technique. However, due to difficulties associated with imposing purely extensional deformations, the development of instrumentation able to carry out extensional viscosity measurements is still a challenging task [17] and even more if we want to analyze the influence of an external electric field aligned with the flow direction.

Among the different techniques developed for characterizing the extensional rheological properties of low viscosity fluids, filament stretching rheometry is considered as an accurate method for characterizing the response of viscoelastic fluids, almost achieving an ideal uniaxial extensional deformation far from the rigid end-plates. The Filament Stretching Extensional Rheometer (FiSER™) and the Capillary Breakup Extensional Rheometer (CaBER™) have showed enhanced performance for rheometric purposes and their relative merits have been discussed thoroughly in [18], but the CaBER™ can be used to measure relaxation times of viscoelastic liquids with significantly lower viscosities than the FiSER™, particularly when the filament thinning process is recorded by a high-speed camera [19]. Very recently, Sadek et al. [20] have developed an electrorheological cell able to apply an external electric field aligned with the direction of extensional flow imposed by the CaBER™, which allows to perform the CaBEER experiments that will provide fundamental information about the suitability of functional inks for the e-jet printing technique.

The present Master Thesis is focused on the development of a COMSOL model that allow for the numerical analysis of the stability/instability mechanisms underlying the extensional flow of magnetic inks under the application of an external electric field.

## 1.2 State-of-the-art

### 1.2.1 E-jet printing

Printing methods depositing functional materials in one single step attract great attention for flexible electronics. Among the plethora of techniques for printed electronics, jet printing-based manufacturing processes are very attractive because of the ability to generate very small-scale droplets, where ink-jet printing using thermal or piezo-excitation represents a highly established and successful approach for the flexible electronic manufacturing, relying on the localized delivery of materials of interest directly to substrates with high spatial control. It demonstrates a group of advantages such as noncontact and additive patterning, minimal waste generation, printability of organics/polymers and inorganic materials, low temperature and inexpensive process, compatible with large area and high-throughput processing. Unfortunately, the conventional inkjet printing is “push” processing, the droplet size is usually several times larger than the nozzle diameter, leading to various intrinsic problems of nozzle blockage, limited ink adaptability and a limited resolution of  $\sim 20 \mu\text{m}$ .

Contrary to such process, the electrohydrodynamic printing (EHD) techniques are “pull” processes as an extra electric field is introduced. By carefully adjusting the ink property, the nozzle-to-substrate distance, and the applied voltage, three types of EHD printing processes can be realized via the same setup (Figure 1.1).

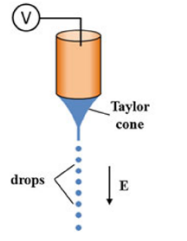
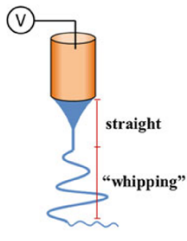
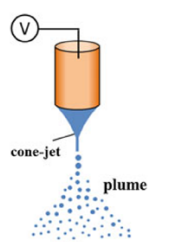
EHD printing	Mode	Voltage (kV)	Electrode distance (mm)	Pattern
E-jet		0.5-3	0.1-1	Dot
Electrospinning		1-15	10-50	Line
Electrospraying		10-30	100-250	Thin film

Figure 1.1: Comparison of the three EHD printing methods. Adapted from Ref. [1].

E-jet printing process is called to be the next-generation of jet printing process, which enables printing of liquid inks with a wide range of viscosity with resolution approaching  $\sim 200$  nm. Thus, E-jet printing represents a high-resolution alternative to conventional thermal and piezoelectric ink-jet systems [13] (Figure 1.2.(a-b)). In e-jet printing systems, ink delivered from a reservoir to the tip of a fine, metal-coated nozzle forms a pendent hemispherical meniscus. A dc voltage bias applied between the nozzle and the substrate leads to the accumulation of mobile charges in the ink near the surface of the meniscus. When a proper electrical potential is employed to the extraction electrode at the outlet of a nozzle, the

liquid droplet would be deformed as the balance of gravity force  $F_g$ , surface tension force  $F_{st}$  and electric field force  $F_e$ , into a conical shape (*Taylor cone*) [21]. With increasing applied voltage, the sum of this electrostatic force and the externally applied pressure eventually exceeds the force associated with the capillary pressure at the apex of the cone, leading to the formation of a thin liquid jet that emerges from the tip of the Taylor cone and ejects toward the substrate [22] (Figure 1.2.(c)).

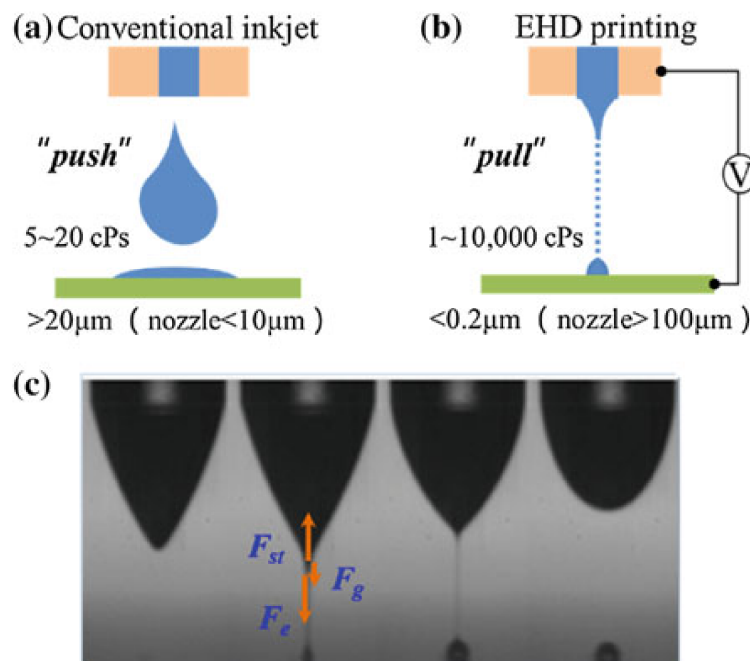


Figure 1.2: Schematic illustration of the conventional ink-jet printing (a) and the e-jet printing (b). The liquid meniscus at the nozzle tip and the evolution of the shape of a Taylor cone during the e-jet printing (c). Reproduced with permission from Ref. [1].

E-jet printing is a very complex process, where the physical properties of the ink controls the formation of the Taylor cone, which is responsible for the generation of stable jets and, ultimately, for the drop generation. The functional inks



consist of a functional material dispersed in a solvent. It has known that the application of external electric field may induce internal microstructures formed by the nanoparticles, and, consequently, affects their rheological properties, namely its viscosity and relaxation time (known as *electrorheological effect*). However, no attention has been given to this circumstance, and both ink parameters (viscosity and relaxation time) are assumed unaltered by the application of an external electric field when determining the printability of functional inks by e-jetting printing.

### 1.2.2 Magnetic inks

The use of magnetic inks in secure printing applications is quite extended among the banking industry to streamline the processing and clearance of cheques and other documents. This magnetic ink contains a magnetic pigment, such as iron oxide, ferrite, magnetite, etc. The printing methods conventionally used for magnetic printing include methods that use a magnetic toner or magnetic ink ribbon, but in recent years, for reasons including printing costs, much development has focused on ink-jet printing methods using a magnetic ink.

The particle size of the magnetic pigment, reported as a median particle size in the dispersed state, is preferably within a range from 10 nm to 200 nm. If the particle size is smaller than 10 nm, then bleeding increases and the magnetic recognition accuracy of characters can sometimes deteriorate. If the particle size exceeds 200 nm, then precipitation of the magnetic particles can sometimes occur, which can induce malfunctioning in the ink-jet head. Additionally, in traditional ink-jet printing process, the aggregation of the magnetic particles causes a change in the ink viscosity that may lead to discharge faults from the ink-jet head too [23].

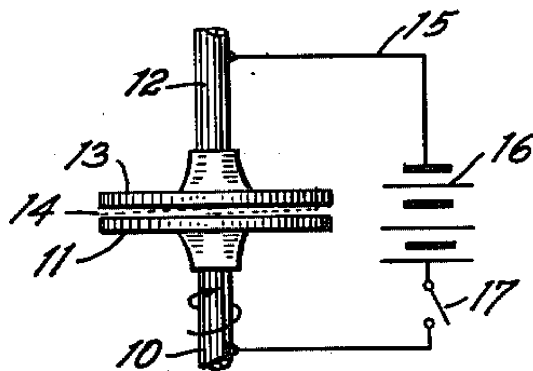


Figure 1.3: An embodiment of an electrorheological clutch proposed by W.M. Winslow in 1947: the power driving shaft (10) provided with a disc (11) translates its movement to a driven shaft (12) via another disc (13) closely spaced and insulated by means of an electrorheological fluid (14), held between them by capillary forces; the two shafts are connected to an electrical circuit (15-17). Image extracted from Ref. [2] via Google Patents.

To the best of the author's knowledge, it has not been explored yet the possibility of using the e-jet printing technique for magnetic printing.

### 1.2.3 Electrorheology

The phenomenon of electrorheology (ER) is related to changes in rheology of suspensions upon the application of electric fields (E) [24]. ER was discovered by A.W. Duff in 1896 when he realized that certain dielectric fluids exhibited a slight reversible change in their viscosity upon the application of an electric field perpendicularly to the direction of the flow [25]. However, it was not until the work of W.M. Winslow, initiated in the 1940s, when the active research on electrorhe-

ological fluids properly begun. For all his contributions, the electrorheological phenomenon is also known as the *Winslow effect* [2, 26, 27, 28] (Figure 1.3).

Electrorheological fluids (ERFs) typically consist of suspensions of very fine particles in an electrically insulating carrier fluid. In the absence of an electric field, the particles are freely suspended in a liquid medium and exhibit properties similar to those of Newtonian fluids. Once an external electric field is activated, the particles aggregate building up fibrous microstructures aligned with the electric field direction [29] (Figure 1.4). That change in the microstructure is reversible once the voltage is removed. ERFs can increase their apparent viscosity by orders of magnitude almost instantaneously upon the application of an electric field, from fluid-like to solid-like, characterized by a yield strength value, which is typically below 10 kPa. This fast, strong and reversible response allows the development of simple and efficient electromechanical systems able to control vibrations and dissipate energy in shocks. However, the weakness of the yield strength delayed the development of many practical applications until the discovery of the Giant ElectroRheological (GER) effect, which can reach a yield strength above the theoretical upper bound on conventional ERFs [30].

ERFs consist of particles dispersed in a carrier fluid, where the polarizable components can be either the fluid or the particles. Nevertheless, most of ERFs reported in the literature consist of a solid phase that can be an inorganic metal oxide, a ferroelectric particle, or some other inorganic/organic polarizable particles suspended in a non-polarizable organic medium [31]. The organic medium can be mineral and silicone oils, halogenated oils and solvents, fluorinated polyethers and polyesters, halogenated polysilicones, and others. The suspension can be stabilized by density matching of the solid and the liquid, by adding surfactants, or by brownian motion in case of using of smaller particles. As the electrorheological phenomena is originated by the dielectric or conductivity mismatch between

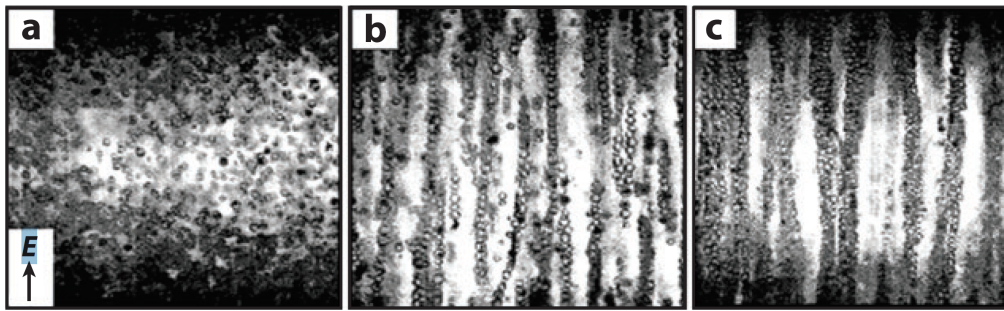


Figure 1.4: ERF consisting of  $1.5 \mu\text{m}$  glass spheres suspended in silicone oil. Structural evolution of dielectric microspheres under an increasing electric field, from (a) no field, to (b)  $500 \text{ V/mm}$ , to (c)  $900 \text{ V/mm}$ . Reproduced from Ref. [3] with permission from The Royal Society of Chemistry.

the particles and continuous phase, the addition of a high dielectric constant additives enabling ionic charge carriers to migrate with the electric field, such as water, carbonates, low molecular weight amines, and alcohols can be used as “activators” to promote the polarizability of the particles [32].

The rheological characterization of electrorheological fluids has been traditionally performed by means of simple shear flow experiments undergone in a rotational rheometer equipped with an electrorheological cell, which allows the application of an external electric field perpendicular to the flow direction. Figure 1.5.(a) shows a rotational rheometer (MCR-301, Anton Paar) equipped with a parallel plate geometry adapted for imposing a vertical electrical field to the fluid sample (ERF); the top plate is connected to a voltage supplier by means of a contact spring, while the bottom plate is connected to ground. Recently, a new electrorheological cell has been developed for the CaBER™ device, allowing to characterize the electrorheological properties of ERFs under extensional flow under the application of an external electric field aligned with the flow di-

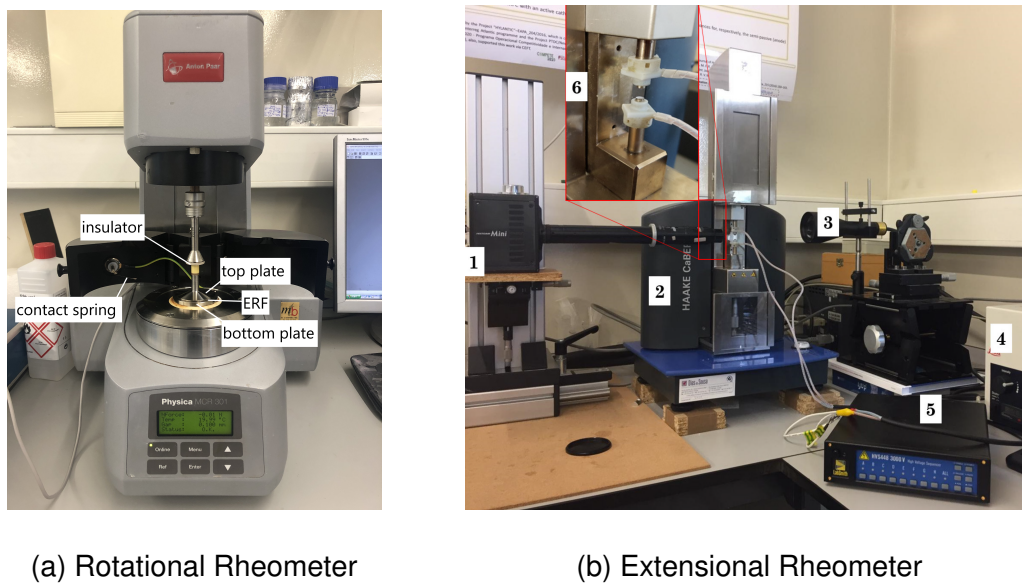


Figure 1.5: Commercial rheometers equipped with electrorheological cells. Reproduced with permission from Ref. [4].

rection [33, 4, 34, 35]. Figure 1.5.(b) shows the Capillary Breakup Extensional Rheometer (2) holding two insulated parallel plates (6) connected to a voltage supplier (5); the silhouette of the filament thinning process is recorded with a high speed camera (1).

Thus, the current state-of-the-art in electrorheology only allows for the characterization of the electrorheological properties of ERFs in two out the four possible flow field Vs electric field configurations; that is, either under shear flow with an electric field perpendicular to the flow or under extensional flow with an electric field aligned to the flow direction (see Figure 1.6).

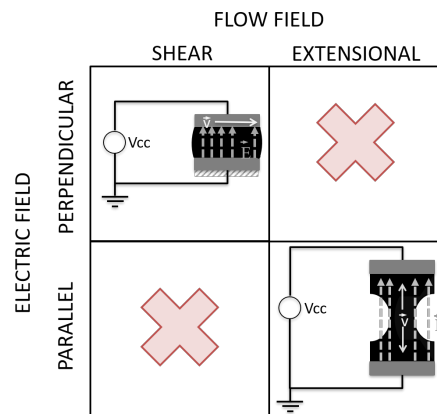


Figure 1.6: Four different flow/electric fields configurations in electrorheometry.

There are many possible free surface conformations that may be considered for understanding the thinning and break-up processes of complex liquids. Three simple prototypical configurations are continuous jetting instability, dripping from a nozzle and necking and breakup of a liquid bridge [5] (Figure 1.7). Thus, it can be considered that the thinning and break-up of a liquid bridge held between two end plates, as used in capillary break-up experiments described in the previous chapter, is equivalent to the break-up of an infinite jet, particularly far from the two end-plates [36]. In this study we assume that the liquid bridge is long and thin so that we can treat it as a slender, axisymmetric jet.

The stability and break-up of liquid jets of Newtonian fluids are now well understood. Surface tension acts to destabilise a liquid jet, driving the free surface to minimise its surface energy and break up into spherical droplets. Viscous forces resist this thinning action and enable the liquid to be drawn into thin, uniform filaments before ultimately breaking up. Eggers developed the theory for the universal pinch off of an axisymmetric free surface, which states that the decay of a Newtonian jet depends on a balance of surface tension ( $\sigma$ ), inertia, and viscosity ( $\mu$ ). This thinning law applies to cases of moderate Ohnesorge number, which is

defined as

$$Oh = \frac{\mu}{\sqrt{\rho\sigma R}}, \quad (1.1)$$

where  $\rho$  is the fluid density and  $R$  is the jet radius. For inkjet printing applications, stable drop generation for Newtonian fluids is limited to a narrow range of viscosities corresponding roughly to Ohnesorge numbers in the range  $0.1 < Oh < 1$ . If the Ohnesorge number is too high, then viscous forces prevent break off of the ligament from the nozzle. On the other hand, if the Ohnesorge number is too low, then surface tension causes the trailing ligament to break up into a number of unwanted satellite drops.

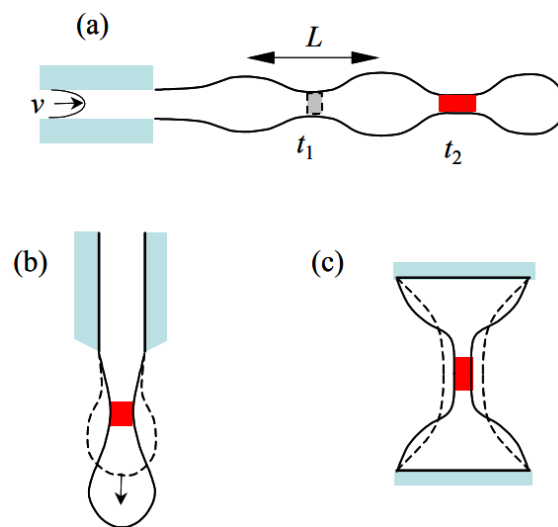


Figure 1.7: Three prototypical geometries for studying breakup of complex fluids; (a) continuous jetting instability; (b) dripping from a nozzle; (c) necking and breakup of a liquid bridge. [5]

The existence of universal thinning laws initiated the use of capillary break-up as a rheological technique. Stretching a liquid sample between two end plates induces a strong extensional flow and thus allows the study of viscous proper-

ties under extensional deformation. Capillary break-up experiments have proved effective in measuring the extensional properties of polymeric fluids, such as relaxation time and extensional viscosity. Furthermore, recent studies have demonstrated that extensional rheometry can be successfully performed on particulate suspensions. However, the detachment dynamics of particle-laden fluids are not yet fully understood [36].

Regarding the e-jet printing process with magnetic inks, it is therefore of paramount importance to study the combined effect of the presence of the particles and the imposed electric field on the stability and breakup of liquid jets; however, this study is yet to be developed.

### **1.3 Objective**

This study represents the first step towards a fundamental understanding of the multiphysics problem of characterizing functional inks by means of capillary breakup extensional electrorheometry (CaBEER). The main objective is providing a precise multiphysic model able to simulate the filament thinning process of functional inks under the presence of an external electric field.

By analysing the stability of a slender, axisymmetric jet we aim at understanding the experimental results obtained in the CaBEER experiments, how the presence of an external electric field affects the movement and self-assembling of the magnetic nanoparticles and, consequently, how this rearrangement results in a macroscopic internal force counterbalancing the filament thinning process driven by capillary forces. This information will be of paramount importance to determine if magnetic inks can be printed out with the electrohydrodynamic jet printing technique.



## 1.4 Methodology

The methodology followed is purely numerical. The CaBEER experimental setup was modeled in Comsol Multiphysics and the fluid sample was considered as a colloidal suspensions of spherical magnetite nanoparticles in a oil phase. By means of the Application Builder, this model is wrapped in an application named as *CaBEER-App*, an easy-to-use interface that would make the simulation of this problem more accessible to a wider audience.

## 1.5 Document structure

In chapter 1 the area of application of this study has been defined. The literature has been reviewed and the objective has been defined in such a way that it enlarges the current state-of-the-art. Finally, the methodology followed in this dissertation has been defined.

In chapter 2 the experimental setup for performing Capillary Breakup Extensional Electrorheometry has been presented, as well as the working fluids.

In chapter 3 the physical model for the Capillary Breakup Extensional Electrorheometry experiments is presented together with a discussion about the physics interfaces available in COMSOL and required in this work.

In chapter 4 a step-by-step description of the implementation of the COMSOL model is presented, as well as the application built for non-expert COMSOL users.

Finally, in chapter 5 the remarks and future works are introduced.



# Chapter 2

## Capillary Breakup Extensional Electrorheometry

### Content

---

2.1 Experimental setup . . . . .	24
2.2 Working fluids . . . . .	25

---

## 2.1 Experimental setup

The experimental setup allowing to perform Capillary Breakup Extensional Electrorheometry is exactly the same as in the CaBER device, but with the application of an electric field (Figure 2.1). The fluid sample is loaded between two parallel discs with diameter  $D_0$  initially separated by a distance  $H_0$ ; at this moment the voltage difference between the two plates is null ( $\Delta V_{cc} = 0$ ). Then the top plate moves vertically in a quasi-step strain manner to the final gap  $H_f$  within the streak time  $t_s \leq 50 \text{ ms}$  and the voltage is set ( $\Delta V_{cc} \neq 0$ ). At that final position, the liquid bridge is not stable and it goes through a self-thinning process until it breaks at the breakup time  $t_b$ . The temporal evolution quantified by the minimum fluid diameter  $d_{min}(t)$  is recorded by an optical device, such as a laser micrometer or a high-speed camera. Finally, the filament thinning data are further processed to extract the material properties of the sample given the selection of a suitable constitutive model [33].

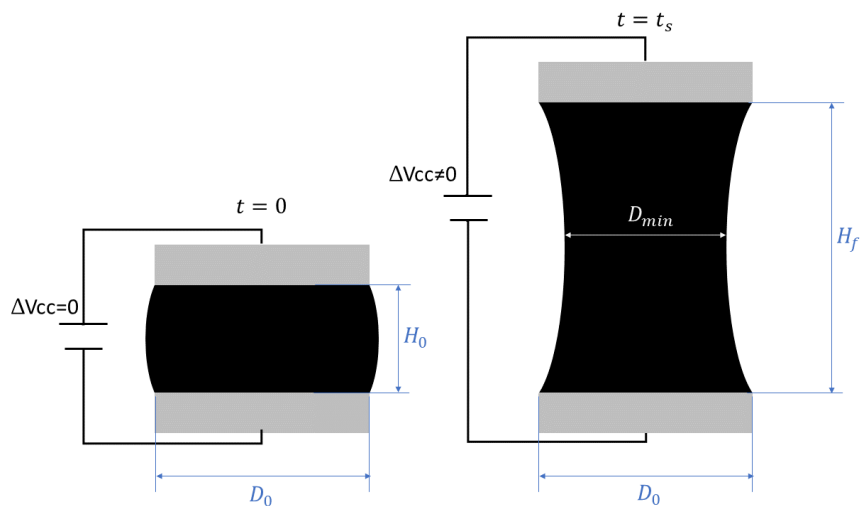


Figure 2.1: Schematic representation of the CaBEER experiment.

During the dynamic capillary-driven process of the liquid bridge between the two end-drops is undergone a uniaxial extensional flow and the radial profile of the liquid bridge is a function of time and the axial position  $R = R(z; t)$ . The structural evolution of the liquid filament is a self-thinning process driven by surface tension and resisted by the viscosity and elasticity of the liquid. The temporal evolution of the mid-plane radius of the liquid bridge  $d_{min}(t)$  captures these self-thinning dynamics and can be used to extract a measure of the transient extensional rheological properties of an unknown material [37].

In the particular case of working with low viscous and low elastic liquids, it has been demonstrated that the above experimental protocol can provide unreliable data due to the presence of fluid inertial effects [38]. Campo-Deaño and Clasen [39] proposed the Slow Retraction Method (SRM), which is a variant of the capillary breakup technique where the top plate moves very slowly beyond the static stability limit, where the liquid bridge reaches the maximum stable slenderness. SRM enables one to create axially symmetric thinning profiles with minimized inertial oscillations from acceleration of the liquid. It is worth to mention here that CaBEER experiments can also be performed by using the SRM protocol.

## 2.2 Working fluids

Ferrofluids are colloidal suspensions of magnetic nanoparticles dispersed in a carrier fluid. Thus, as ferrofluids perfectly matches the definition given in Section 1.2.2 for magnetic inks, in this study we will consider commercial ferrofluids as working fluids for this study. Particularly, the formulation of oil-based ferrofluids from Ferrotec Inc. (EMG905) will be used in this study to define the working fluids.

The nominal size of the magnetic particles in all the fluids is 10 nm. The magnetic nanoparticle is majoritarian of magnetite ( $Fe_3O_4$ ), but according to Ieta, et al. [40] some maghemite ( $Fe_2O_3$ ) may also be found. The supplier [41] provided with the following information:

- Carrier liquid - Light Hydrocarbon Oil,
- Viscosity of 6 mPa · s at 27 °C.
- Saturation magnetization - 44 mT,
- Initial magnetic susceptibility  $\sim 3.52$  .
- Density - 1200 kg/m<sup>3</sup>.
- Magnetic particle concentration 7.8 % by volume.
- Dispersant - Oleic Acid

The surface tension ( $\sim 23$  mN/m) was measured by means of a force tensiometer (Attension Sigma 700/701, Biolin Scientific) equipped with a Platinum-Iridium Du Nouy ring at 22 °C.

Regarding the electrical properties of ferrofluids, the dielectric behavior of ferrofluid changes with the application of an external field and with the relative orientation of the electric and magnetic fields. This effect is known as magneto-dielectric anisotropy effect [42]. In the absence of an electric field, a ferrofluid is a homogeneous suspension and the field-induced magneto-dielectric effect can be neglected. However, the magnetic nanoparticles in a ferrofluid are polarizable and dielectric spectroscopy allows to determine their dielectric parameters.

Basaran and Wohlhuter [43] reported that ferrofluids exhibited a nonlinear polarization that follows a Langevin equation of the form:

$$P = \alpha \left[ \coth(E\tau) - \frac{1}{E\tau} \right] \quad (2.1)$$

where  $E$  is the electric field strength, and  $\alpha$  and  $\tau$  are the Langevin parameters. The Langevin equation is considered the simplest form of a constitutive equation frequently used to describe the polarizability of magnetically susceptible fluids. It has been demonstrated that the form of the equations that govern the response of a drop of dielectric liquid in an applied electric field is the same as those that govern the response of a drop of ferrofluid in an applied magnetic field [43].

Preliminary CaBEER experiments revealed that there is a critical electric field beyond which the filament thinning process of oil-based ferrofluid EMG905 changes from Newtonian-like to viscoelastic-like behaviour (Figure 2.2).

Figure 2.2: Time evolution of the minimum diameter of the ferrofluid EMG905 obtained in CaBEER experiments (reproduced with permission from [6]).

In this study we want to provide a Comsol model that allow to investigate the importance of the different parameters affecting the change in the rheological behavior of ferrofluids undergone to an extensional flow aligned with the electric field, as we suspect that experimental observed change in the filament thinning process is connected with the development of microstructures in the magnetic ink due to the polarization of the magnetic nanoparticles. This numerical tool will allow to get relevant information to the practical application of magnetic inks by electrohydrodynamic jet printing technique.





# Chapter 3

## Modelling

### Content

---

<b>3.1 Introduction</b> . . . . .	<b>30</b>
<b>3.2 Model Definition</b> . . . . .	<b>32</b>
<b>3.3 Problem formulation</b> . . . . .	<b>33</b>
3.3.1 Two-phase Flow, Phase field . . . . .	33
3.3.2 Electrostatic . . . . .	36
3.3.3 Particle Tracing for Fluid Flow . . . . .	38
3.3.4 Initial and boundary conditions . . . . .	43

---

### 3.1 Introduction

The filament thinning and break-up processes of functional inks under the application of an external electric field aligned with the extensional flow is modeled. As mentioned before, this phenomenon is driven by surface tension. Gradients in the surface tension originated by gradient of the temperature in the liquid thread would lead to Marangoni effect [44], which introduces a force acting only in the tangential direction on the interface that must be counterbalance by viscous forces present in the liquid sample. Eventually, the tangential force turn the liquid filament unstable and the thinning process is triggered. However, in the CaBEER experiments (Chapter 2), the temperature across the liquid sample and surrounding air is constant and so it is the surface tension. In that case, the stability of the two-fluid system depend on the aspect ratio  $\Lambda = \frac{L}{2R}$  of the filament and the Bond number ( $Bo = \frac{\rho g R}{2\sigma}$ ), which captures the effects of gravity against the surface tension  $\sigma$  and is a measure of how much the initial cylindrical filament ‘sags’. For a given Bond number, there is a critical aspect ratio above which the liquid bridge becomes unstable [7] (Figure 3.1); thus, the larger the Bond number the more sagging and smaller critical aspect ratios. This is the basis of the Slow Retraction Method [39].

In the absence of any external field (nor electric nor magnetic), the mere presence of particles dispersed in the liquid phase increases its bulk viscosity and, consequently, it is expected to retard thinning and consequently delay the time to break-up [45]. However, it has been experimentally observed that presence of micron-sized particles alters the pinch-off dynamics of a liquid bridge and the thinning no longer follows the behaviour predicted by the bulk viscosity; instead, the thinning process is “accelerated” by increasing particle-density fluctuations

that generate locally diluted zones. The final thinning dynamics return to the self-similar scaling of a viscous Newtonian liquid bridge in the final moments preceding breakup [36, 46].

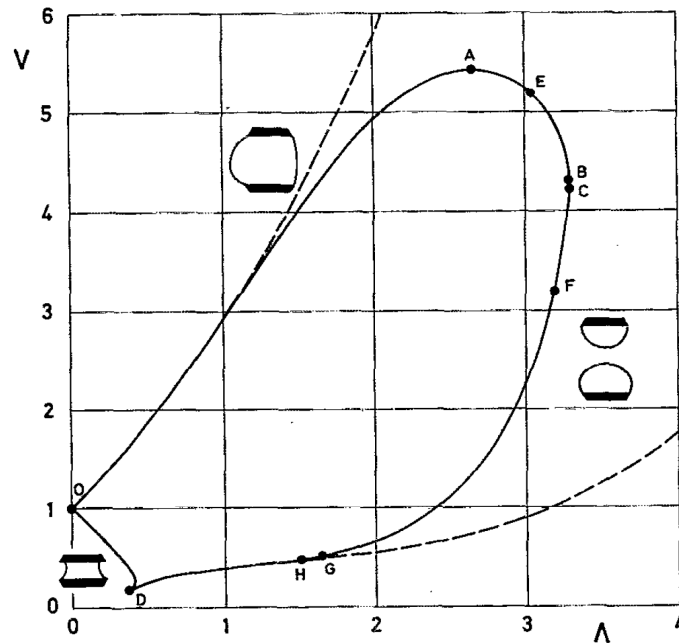


Figure 3.1: Typical stability diagram of liquid bridges between equal disks subjected to a small constant axial acceleration [measured by Bond number:  $Bo = 0.1$  (solid line),  $Bo = 0$  (dashed line)]. Reprinted from [7], with the permission of AIP Publishing.

In this work a numerical multiphysics model for the thinning and breakup process functional magnetic inks (nanoparticle-laden liquid) under the presence of an external electric field is proposed.

## 3.2 Model Definition

A liquid jet surrounded by air is modelled by a fluid domain in 2D, considering the axis of symmetry of the liquid phase. A cylindrical fluid domain with radius  $R_d$  and length  $L$  contains an initial cylinder of liquid sample with radius  $R_l$  (Figure 3.2). The liquid sample consist of a Newtonian liquid carrying magnetic nanoparticles with a nominal diameter of  $D_p \sim 10 \text{ nm}$ ; while the surrounding gas phase is air.

The liquid phase is undergone to an external applied field that results from imposing a voltage difference  $\Delta V_0$  between top and bottom contours. As the liquid sample is dielectric, the presence of electric currents is neglected.

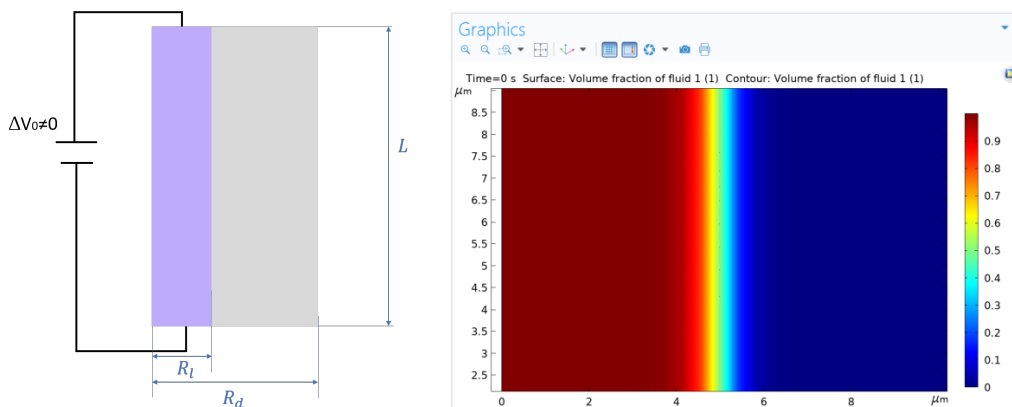


Figure 3.2: Fluid domain (left), where the liquid phase is highlighted in purple; and fluid interface (right), where the liquid sample is in red ( $V_f = 1$ ), the gas phase is in blue ( $V_f = 0$ ) and the interface is a band around  $V_f = 0.5$ .

## 3.3 Problem formulation

This is a clear example of a multiphysics problem in which we have coupled several multiphysics modules from Comsol:

- **Two-Phase Flow, Phase Field**, where the *laminar flow* interface is coupled with the *Phase Field* physics interface so that the phase boundary between the two immiscible fluids can be determined accurately.
- **Fluid-Particle Interaction**, where the *laminar flow* physics interface is coupled with the *Particle Tracing for Fluid Flow* interface, so that the effect of the movement of the nanoparticles into the laminar flow of the liquid sample is taken into account.

The presence of the magnetic nanoparticles in the liquid sample will be modeled with the *Particle Tracing for Fluid Flow* interface, which will account for all the forces acting on the particles, i.e. Brownian force, gravity, drag and the force due to the induced dipolar moment. In order to consider this latter force, the *Electrostatic* physics is also required, which will allow to impose the electric field in the liquid domain.

### 3.3.1 Two-phase Flow, Phase field

In order to validate the model with experimental results, it is very important to describe the phase boundary in detail. Therefore, a separated multiphase flow model is preferred to a dispersed multiphase flow model. In both approaches, a function  $\Phi$ , is used to describe the presence of the gas and liquid phases;

however, in the separated multiphase flow models, the different phases are exclusive, and there is a sharp phase boundary between them where the phase field function  $\Phi$  changes abruptly. The phase field function does not have a physical meaning other than keeping track of the location of the phase boundaries [47].

There are three different interface tracking methods in the COMSOL Multiphysics software for separated multiphase flow models, i.e. *moving mesh*, *level-set* and *phase-field*. Among them, the latter one was preferred for two reasons:

1. Topology changes are expected.
2. Surface tension effects are important.

Thus, the liquid sample and the surrounding gas are separated by a fluid interface that is tracked in detail, including surface curvature and surface tension forces. The phase-field method use a fixed background mesh and solve additional equations to track the interface location.

The velocity field and pressure for the liquid phase are described by the mass conservation equation (Equation 3.1) and the momentum balance equation (Equation 3.2), known as governing equations<sup>1</sup>. These equations have been simplified considering that in this process both fluids are incompressible ( $\rho = cte$ ).

$$\nabla \cdot \mathbf{v} = 0, \quad (3.1)$$

$$\rho \frac{\partial \mathbf{v}}{\partial t} + \rho (\mathbf{v} \cdot \nabla) \mathbf{v} = \nabla \cdot \left[ -p\mathbf{I} + \mu \left( \nabla \mathbf{v} + (\nabla \mathbf{v})^T \right) \right] + \mathbf{F}_{st} + \rho \mathbf{g} + \mathbf{F}_e, \quad (3.2)$$

---

<sup>1</sup>As the filament thinning process is isothermal, the equation of energy can be decoupled from these two governing equations and, consequently, it is not taken into consideration in this model.

where  $\mathbf{v}$  is the fluid velocity,  $\rho$  is the density,  $\sigma$  is the surface tension,  $\mu$  is the viscosity,  $\mathbf{F}_{st}$  is the force due to the surface tension,  $\mathbf{g}$  is the gravitational acceleration<sup>2</sup>, and  $\mathbf{F}_e$  is the volumetric electric force.

In the *phase field* method to track the fluid-fluid interface adds the following equations [48]:

$$\frac{\partial \Phi}{\partial t} + \mathbf{v} \cdot \nabla \Phi = \nabla \cdot \frac{\gamma \lambda}{\epsilon^2} \nabla \Psi, \quad (3.3)$$

$$\Psi = -\nabla \cdot \epsilon^2 \nabla \Phi + (\Phi^2 - 1) \Phi + \left( \frac{\epsilon^2}{\lambda} \right) \frac{\partial f_{ext}}{\partial \Phi} \quad (3.4)$$

where  $\lambda$  is the mixing energy density and  $\epsilon$  is a capillary width that scales with the thickness of the interface. These two parameters are related to the surface tension coefficient ( $\sigma$ ) through the following equation:

$$\sigma = \frac{2\sqrt{2}}{3} \frac{\lambda}{\epsilon}, \quad (3.5)$$

and  $\gamma$  is related to  $\epsilon$  through  $\gamma = \chi \epsilon^2$ , where  $\chi$  is the mobility tuning parameter.

Once  $\Phi$  is calculated, the volume fraction of the gas phase is computed as follows (Figure 3.2:

$$V_f = \min(\max([1 + \Phi]/2, 0), 1), \quad (3.6)$$

where the min and max operators are used so that the volume fraction has a lower limit of 0 and an upper limit of 1. The fluid properties are then defined as a function of  $V_f$ :

$$\rho = \rho_l + (\rho_l - \rho_g) V_f \quad (3.7)$$

$$\mu = \mu_l + (\mu_l - \mu_g) V_f \quad (3.8)$$

$$\epsilon = \epsilon_l + (\epsilon_l - \epsilon_g) V_f \quad (3.9)$$

---

<sup>2</sup>In this study, we leave open the possibility of having a non-negligible density difference between the two phases.

The mean curvature is calculated according to the following expression:

$$\kappa = 2(1 + \Phi)(1 - \Phi) \frac{G}{\sigma}, \quad (3.10)$$

where  $G$  is the chemical potential defined as

$$G = \lambda \left( -\nabla^2 \Phi + \frac{\Phi(\Phi^2 - 1)}{\epsilon^2} \right) + \frac{\partial f}{\partial \Phi} \quad (3.11)$$

The surface tension force ( $\mathbf{F}_{st}$ ) in the *phase field* method is implemented as a body force:

$$\mathbf{F}_{st} = \left( G - \frac{\partial f}{\partial \Phi} \right) \nabla \Phi, \quad (3.12)$$

where the term  $\frac{\partial f}{\partial \Phi}$  is a user-defined source of free energy, which has been set to 0 in this model.

### 3.3.2 Electrostatic

In this model, the fluid domain consist of a colloidal suspension of magnetic nanopartiles in a light hydrocarbon oil similar to kerosene, having a charge relaxation time  $\sim 0.1s$  [49], which more than 1000 times larger than the characteristic time of the filament thinning process without the application of an external field. Therefore, the charges do not have time to redistribute to any significant degree. Thus the charge distribution can be considered as a given model input. The best approach is to solve the Electrostatics formulation using the electric potential  $V$  [50].

By combining the definition of the potential with Gauss' law, the classical Poisson's equation can be derived. Under static conditions, the electric potential  $V$  is defined by the equivalence  $\mathbf{E} = -\nabla V$ . Using this together with the constitutive relation  $\mathbf{D} = \epsilon_0 \mathbf{E} + \mathbf{P}$  between the electric field ( $\mathbf{E}$ ) and the electric displacement ( $\mathbf{D}$ ), the Gauss' law can be rewritten as a variant of Poisson's equation:



$$-\nabla \cdot (\epsilon_0 \nabla V - \mathbf{P}) = \rho_c, \quad (3.13)$$

where  $\epsilon_0$  is the permittivity of vacuum,  $\mathbf{P}$  is the electric polarization vector and  $\rho_c$  is the space charge density. This equation describes the electrostatic field in dielectric materials.

This equation is used in the Electrostatics interface. It is worth noting that Gauss' law does not require the charge distribution to be static. Thus, provided dynamics are slow enough that induced electric fields can be neglected and hence a scalar electric potential is justified, the formulation can be used also in the Time Dependent study type. That typically involves either prescribing the charge dynamics or coupling a separate formulation for this.

The axisymmetric version of the physics interface considers the situation where the fields and geometry are axially symmetric. In this case, the electric potential is constant in the  $\phi$ -direction, which implies that the electric field is tangential to the  $rz$ -plane.

As mentioned in Section 2.2, the magnetic nanoparticles dispersed in a light hydrocarbon oil are polarizable. The ferroelectricity phenomenon is related to phase transitions in materials. In its ferroelectric phase, the material exhibits spontaneous polarization, so that it is constituted of domains with nonzero polarization even at zero applied field. This is similar to permanent magnetism in ferromagnetics, which explains the name used for such materials. Application of an electric field can rearrange the domains resulting into the net polarization in the material. At very large electric fields, the polarization saturates, as all ferroelectric domains in the material are aligned along the direction of the applied field. Domain wall interactions can also lead to a significant hysteresis in the polarization.

All domains are assumed to have polarization of the same magnitude  $P_s$ , but the polarization can have different orientations. The applied electric field changes the domain orientation, and the resulting net polarization in the ferroelectric material is found from the following nonlinear implicit relation:

$$\mathbf{P} = P_s L(|\mathbf{E}_{eff}|) \frac{\mathbf{E}_{eff}}{|\mathbf{E}_{eff}|}, \quad (3.14)$$

where the effective field in the material is given by

$$\mathbf{E}_{eff} = \mathbf{E} + \alpha \mathbf{P}, \quad (3.15)$$

being the matrix  $\alpha$  the term characterizing the inter-domain coupling. The polarization shape is characterized by the function  $L$  with the following properties:

- For weak effective fields, the polarization is nearly linear  $\mathbf{P} \approx \chi_0 \mathbf{E}_{eff}$  and it can be characterized by the initial electric susceptibility matrix  $\chi_0$ .
- For strong fields, the polarization magnitude approaches the saturation value  $\mathbf{P} \approx P_s \frac{\mathbf{E}_{eff}}{|\mathbf{E}_{eff}|}$ . There are two possibilities for the polarization shape: a) the Langevin function  $L = \coth\left(\frac{3\chi_0 |\mathbf{E}_{eff}|}{P_s}\right) - \frac{P_s}{3\chi_0 |\mathbf{E}_{eff}|}$ , or b) the hyperbolic tangent  $L = \tanh\left(\frac{\chi_0 |\mathbf{E}_{eff}|}{P_s}\right)$ . As mentioned above, Basaran and Wohlhuter [43] reported that ferrofluids exhibited a nonlinear polarization that follows a Langevin equation.

### 3.3.3 Particle Tracing for Fluid Flow

The fact of working with a colloidal suspension forces us to carefully study the interaction and behavior of the nanoparticles during the fluid flow process, because a correct understanding of its internal interactions is of paramount importance to understand the unusual filament thinning process observed in Figure 2.2. By

controlling the inter-particle force, weak or strong particle aggregates can be produced within the magnetic ink. The colloidal stability of the ink depends on the total inter-particle potential energy, which is obtained from the sum of the potential energy due to the long-range Van der Waals attractive forces between the particles and the potential energy due to the electrical repulsive force resulting from identical electrical charges on the colloidal particles. As the ink is stable with out the application of any external field, the effect of this inter-particle force is neglected in this model. On the contrary, the inter-particle force due to the induced dipolar momentum by the presence of the electric field will be considered here.

The potential energy of a rigid dipole ( $\mathbf{p}_1$ ) undergone to the electric field produced by another dipole ( $\mathbf{p}_2$ ) located at a distance  $r$  is given by the following expression:

$$W_{dd} = \frac{1}{4\pi\epsilon_0} \left[ \mathbf{p}_1 \cdot \mathbf{p}_2 - \frac{3}{r^2} (\mathbf{p}_1 \cdot \mathbf{r}) (\mathbf{p}_2 \cdot \mathbf{r}) \right], \quad (3.16)$$

which allows to calculating the force between them as  $\mathbf{F}_{dd} = -\nabla W_{dd}$ :

$$\mathbf{F}_{dd} = \frac{15 (\mathbf{p}_1 \cdot \mathbf{r}) (\mathbf{p}_2 \cdot \mathbf{r})}{4\pi\epsilon_0 r^7} \mathbf{r} - \frac{3 [\mathbf{p}_1 (\mathbf{p}_2 \cdot \mathbf{r}) + \mathbf{p}_2 (\mathbf{p}_1 \cdot \mathbf{r}) + \mathbf{r} (\mathbf{p}_1 \cdot \mathbf{p}_2)]}{4\pi\epsilon_0 r^5}, \quad (3.17)$$

where the dipolar momentum  $\mathbf{p}_i$  is calculated as mentioned in Section 3.3.2.

Besides the inter-particle force due to the polarization of the nanoparticles in the presence of the electric field, each particle is undergone to three external forces, i.e. Brownian force, drag force and gravitational force (Figure 3.3) [45]:

- **Brownian force** ( $\mathbf{F}_B$ ). The fundamental unit of energy in the colloidal world is the thermal energy  $k_B T$ , where  $k_B$  is Boltzmann's constant and  $T$  is the absolute temperature ( $T$ ). Although this energy appears to be small, it sets the energy scale for all colloidal interactions:

$$\mathbf{F}_B = \zeta \sqrt{\frac{6\pi k_B \mu T d_p}{\Delta t}}, \quad (3.18)$$

where  $\mu$  is the dynamic viscosity of the surrounding fluid,  $\Delta t$  is the time step taken by the solver, and  $\zeta$  is a dimensionless normally distributed random number with a mean of zero and unit standard deviation.

- **Drag force ( $F_D$ )**, Considering the low Reynolds number in the thinning flow process, the Stokes drag law can be used to get the drag force for each particle as follows:

$$F_D = 3\pi\mu d_p (\mathbf{u} - \mathbf{v}), \quad (3.19)$$

where  $\mathbf{u} - \mathbf{v}$  is the relative velocity between the fluid and the particle.

- **Gravitational force ( $F_g$ )**. This force comes from the density mismatch between the particle and the surrounding fluid and is given by:

$$F_g = \frac{(\rho_p - \rho_l) \pi d_p^3}{6} g \quad (3.20)$$

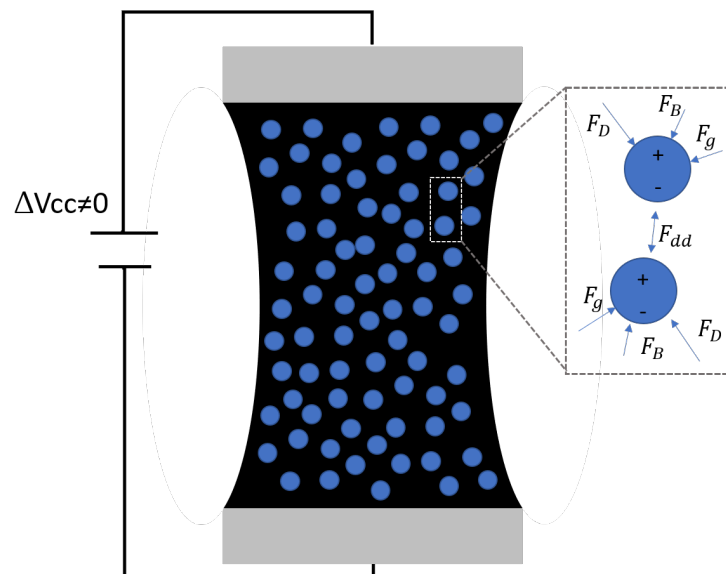


Figure 3.3: Schematic representation of the ink filament containing the colloidal particles undergone to the particle-particle force due to the induced dipoles and the three external forces (Brownian, drag and gravitational).

Particle tracing [51] provides a Lagrangian description of a problem by solving ordinary differential equations using Newton's law of motion. The trajectories of individual particles are always solved for in the time domain. Newton's law of motion requires specification of the particle mass and all forces acting on the particle. The forces acting on particles may be due to external fields which can be specified directly or computed using a different physics interface, often using the Finite Element Method (FEM). For each particle, a second-order ordinary differential equation is solved for each component of the position vector. This means that two ordinary differential equations are solved for each particle in our problem, which is 2D. At each time step taken by the solver, the forces acting on each particle are queried from the external fields at the current particle position. If particle-particle interaction forces are included in the model then they are added to the total force. The particle position is then updated and the process repeats until the specified end time for the simulation is reached. During each time step, the particles may interact with boundaries in the geometry, or they may be subjected to other phenomena that can discontinuously change the particle velocity.

When modeling the motion of small particles in a fluid, it is important to first evaluate whether particle inertia is important enough to be included in the model. Particle inertia can be seen as a velocity lag, where larger and heavier particles change direction only gradually when the surrounding fluid changes direction, whereas smaller particles will start to match the surrounding fluid velocity almost immediately. Particle inertia is most significant when the model particles are large and heavy, or when the surrounding fluid has very low viscosity, or a combination of the two. In our case, even when the particle size is very small, due to the fact that the magnetic nanoparticles are heavier than the carrier fluid, which viscosity is very small, and they can form chains due to their polarization, leading to a larger effective particle size, the inertia of the particles will be considered by

selecting the Newtonian formulation in the physics interface Particle Release and Propagation section.

In a dilute flow the continuous phase affects the motion of the particles and the particle motion in turn disrupts the continuous phase. This is often referred to as a bidirectional coupling. The bidirectional coupling between particles and fluids can be modeled using the Fluid-Particle Interaction multiphysics coupling node. The body force exerted on the fluid by the particle is applied in an approximate way, in that it is smeared out over a mesh element. This smearing effect makes the volume force computed by the Fluid-Particle Interaction node somewhat mesh dependent.

The advective transport of particles due to drag and other applied forces is usually deterministic, meaning that any number of particles released from the same point and with the same initial velocity would follow the same trajectory. Sometimes particle motion also includes a diffusive component, by which particles tend to spread out over time. The Brownian Force is most significant when the particles are extremely small, generally in the sub-micron range. Brownian motion causes particles to drift because the number of molecules striking each particle from different sides is random, since the molecules in a fluid (even at room temperature) move around randomly and at high speeds. When the particles are larger, Brownian motion is less of a driving factor because the number of molecules hitting the particle surface is large enough that they tend to average out more readily.

### 3.3.4 Initial and boundary conditions

Initially, both fluids are at rest. Thus, both fluid velocities are null and the magnetic nanoparticles are only under the action of the Brownian motion and the gravitational force. The fluid is considered to be an homogeneous dispersion of magnetic nanoparticles.

In order to minimize the computational time and cost, an axisymmetric 2D computational domain model that uses cylindrical coordinates is used. Periodic boundary conditions are imposed on the top and bottom boundaries to mimic the effect of the jet being infinitely long in length:

$$\mathbf{v}_{top} = \mathbf{v}_{bottom}, \quad (3.21)$$

$$p_{top} = p_{bottom}, \quad (3.22)$$

$$\Phi_{top} = \Phi_{bottom} \quad (3.23)$$

The outer contour of the gas phase is modelled as a wall with no slip condition and containing a point where the pressure is constrained to make the pressure unique.





# Chapter 4

## Implementation, results and discussion

### Content

---

<b>4.1 Two-phase Flow . . . . .</b>	<b>46</b>
<b>4.2 Particle Tracing for Fluid Flow . . . . .</b>	<b>53</b>
4.2.1 External forces . . . . .	55
4.2.2 Inter-particle force . . . . .	57
<b>4.3 CaBEER model . . . . .</b>	<b>59</b>
<b>4.4 CaBEER-APP . . . . .</b>	<b>61</b>

---

As discussed in the previous chapter, the filament thinning process of a magnetic ink under the presence of an external electric field aligned with the flow is a complex problem to model and so it is its implementation in Comsol Multiphysics. Thus, the *divide and conquer* approach was followed: First, the two-phase fluid flow model was built-up; then, separately, a new model considered either exclusively the external forces acting on the magnetic nanoparticles or the inter-particle force coming from the induced dipoles; finally, all these features were put in place in the *CaBEER.mph* model, which was complemented with a simulation APP.

## 4.1 Two-phase Flow

This model is contained in the file *CaBEERTwoPhaseFlow.mph* (Figure 4.1).

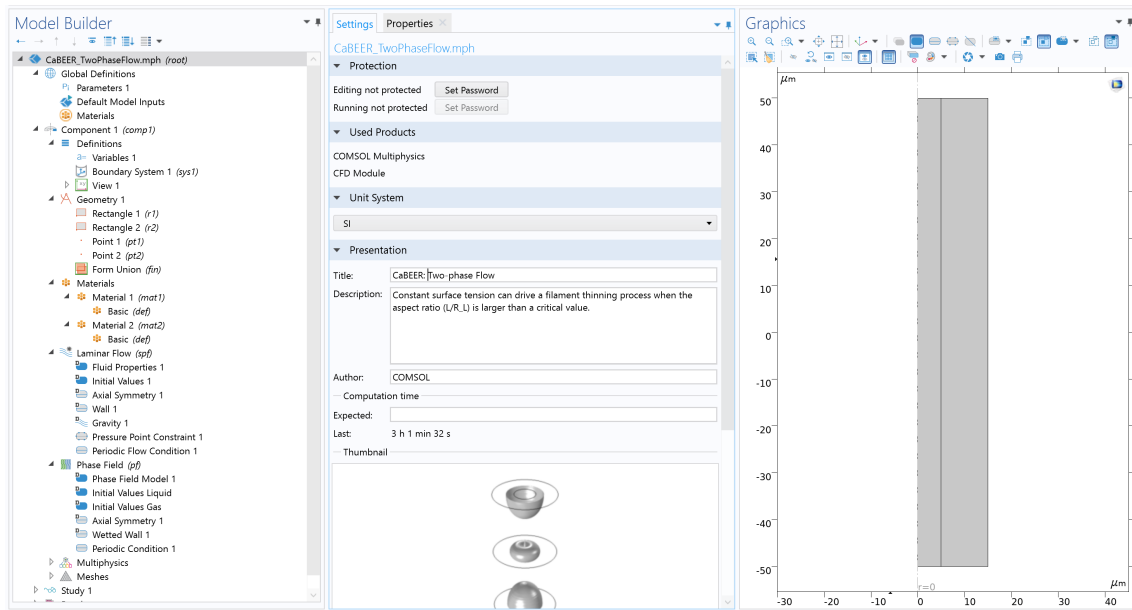


Figure 4.1: Printscren showing the general view of the Two-Phase Flow model.

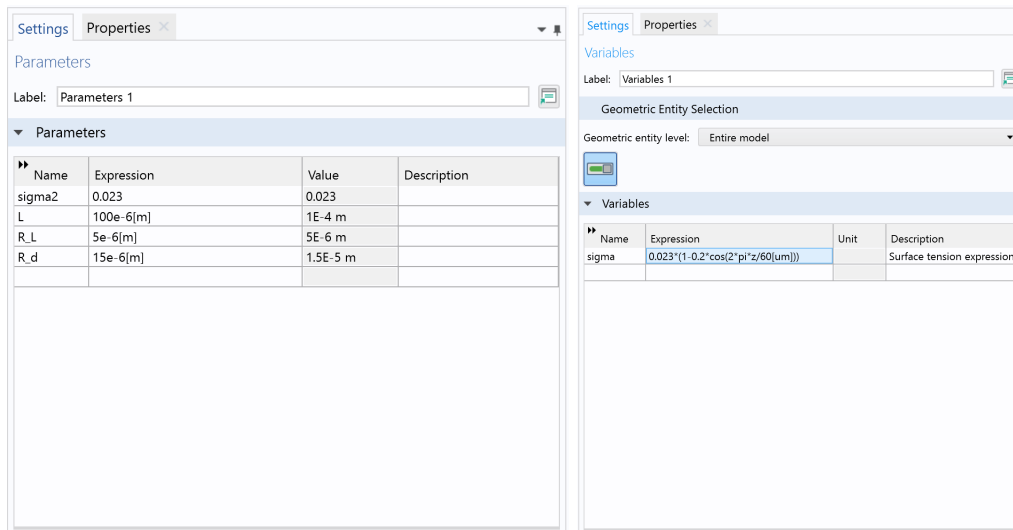


Figure 4.2: Definition of geometric parameters and surface tension, either as a constant parameter or as a variable if Marangoni effect were intended to be simulated.

The geometric parameters referring to the fluid domain ( $L$ ,  $R_L$  and  $R_d$ ) were defined together with a constant surface tension value<sup>1</sup> (Figure 4.2). The fluid domains are assigned with two materials, which viscosity and density are user-defined (Figure 4.3). Then, the *Laminar Flow* interface is configured for incompressible Newtonian fluids, considering gravitational effects and for a reference temperature of 293.15 K (Figure 4.4). Additionally, the initial and boundary conditions are set as indicated in the previous chapter.

<sup>1</sup>The possibility of considering Marangoni effect was also left open, by defining a surface tension dependent on the z-position as variable:  $sigma = 0.023(1 - 0.2 \cdot \cos(2\pi z/L))$ .

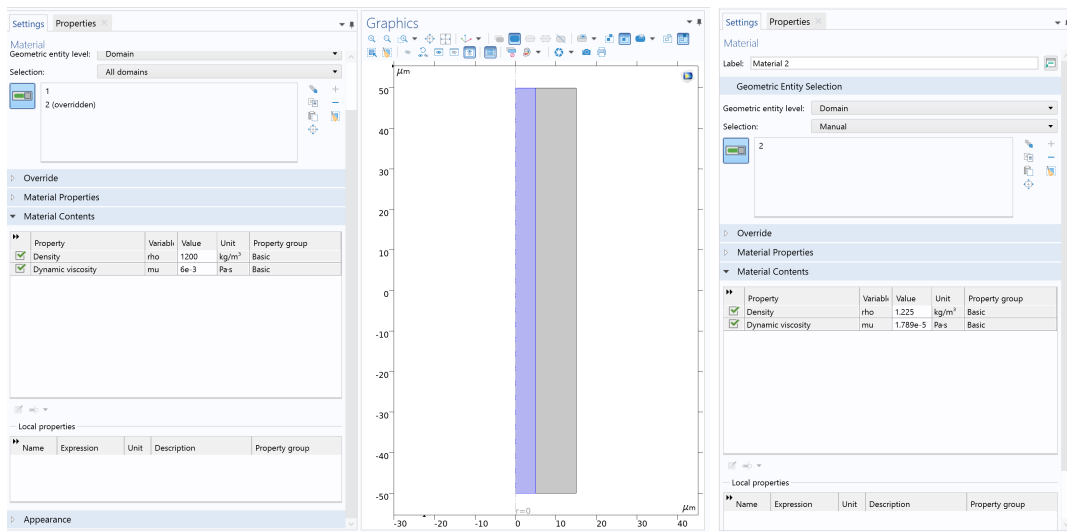


Figure 4.3: The viscosity and density of the two fluids are defined as material properties: liquid in purple (left) and gas in grey (right).

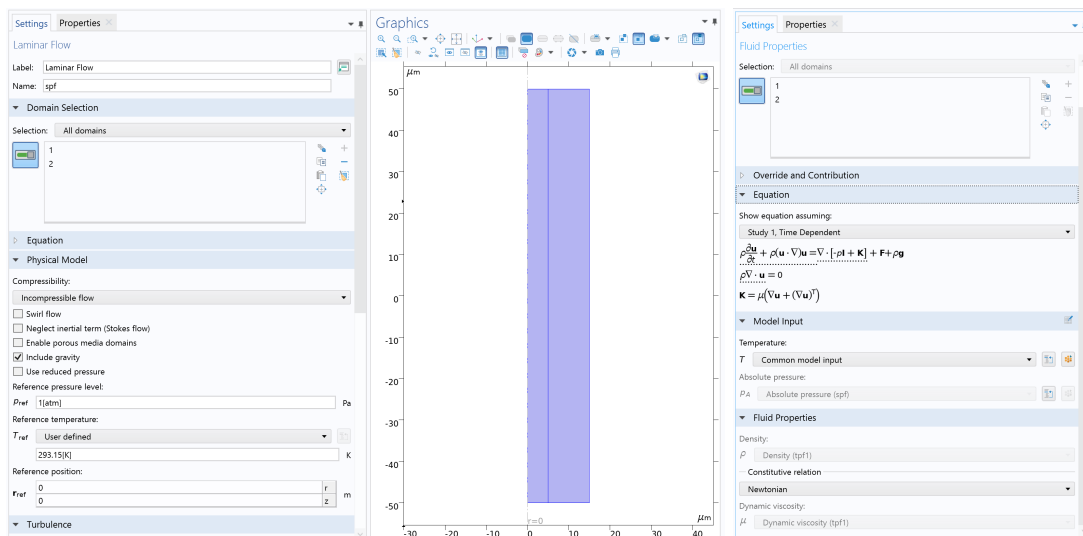


Figure 4.4: Definition of the Laminar flow interface.

Now, the *Phase Field* interface is defined (Figure 4.5), including the width of the interphase ( $\epsilon_{pf}$ ), the initial domains for liquid ( $\Phi = -1$ ) and gas ( $\Phi = 1$ ), as well as the boundary conditions as defined in the previous chapter.

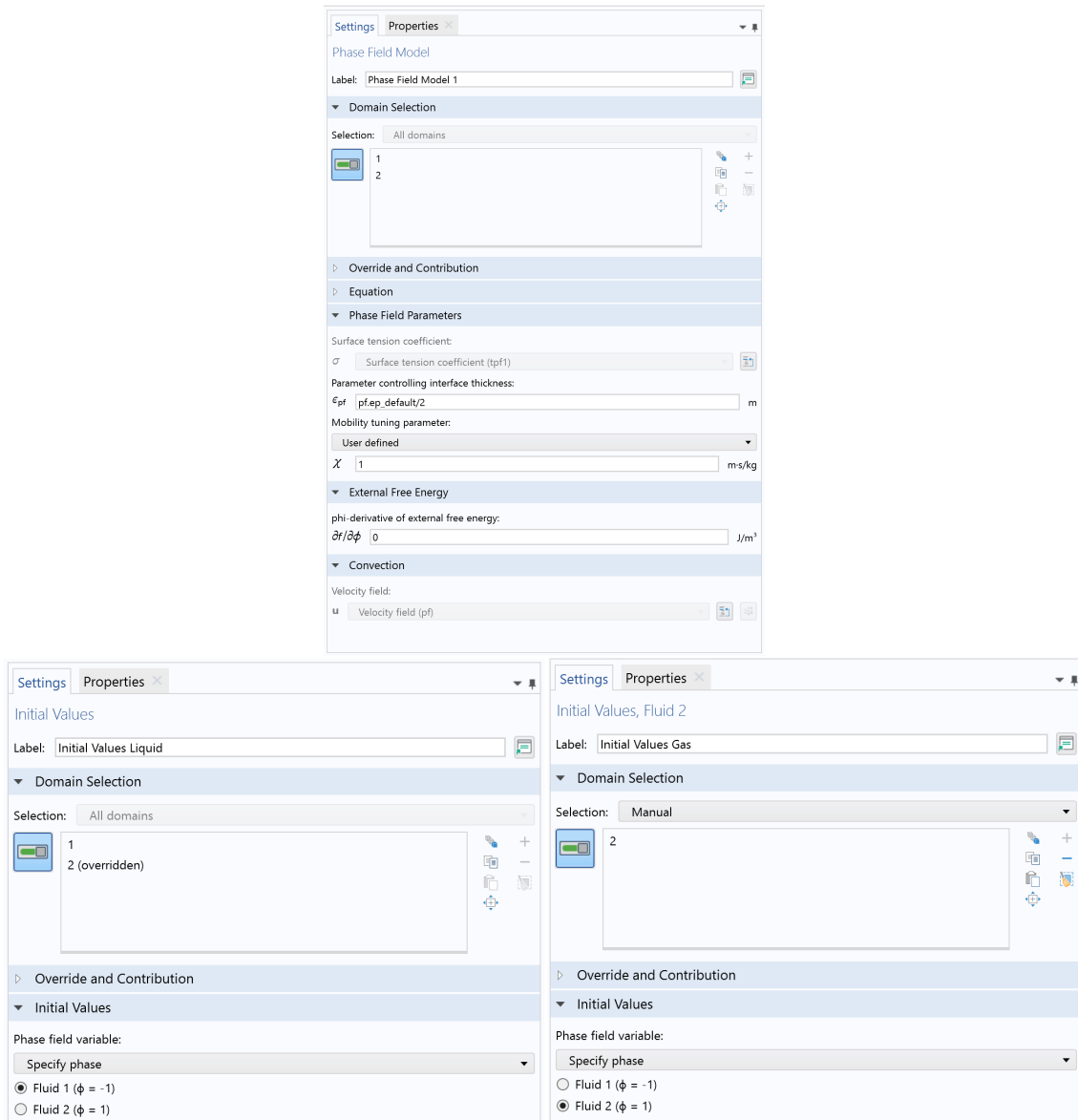


Figure 4.5: Definition of the Phase Field interface.

Finally, the two physics above are coupled by means of the multiphysics inter-

face *Two-Phase Flow, Phase Field* (Figure 4.6), where it is set that the fluid flow is solved with Laminar Flow interface while the moving interface is solved with the Phase Filed interface; the temperature is a common model input; the fluid density and viscosity of each domain are taken from the defined materials, while the surface tension is taken from the designed parameter. In order to solve the coupled problem, a time dependent study with a initialization phase is added (Figure 4.7). In the first step, the phase field in the stationary; then, the time dependent step solves numerically the coupled problem by using adaptative mesh refinement and a PARDISO solver for both the flow and phase field variables.

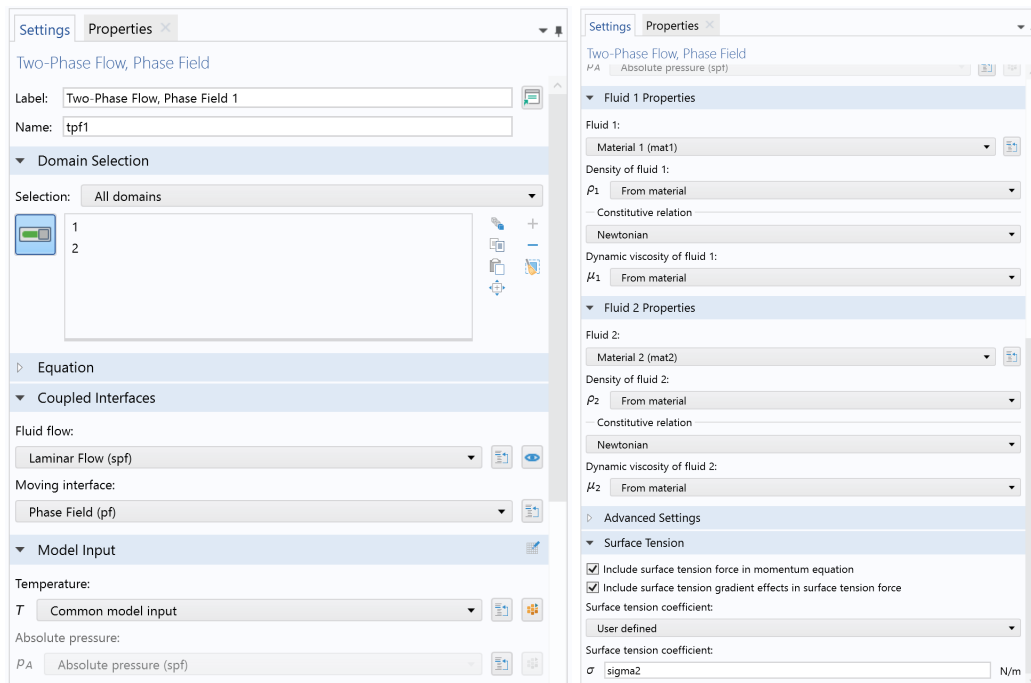


Figure 4.6: Definition of the Multiphysics *Two-Phase Flow, Phase Field* coupling.

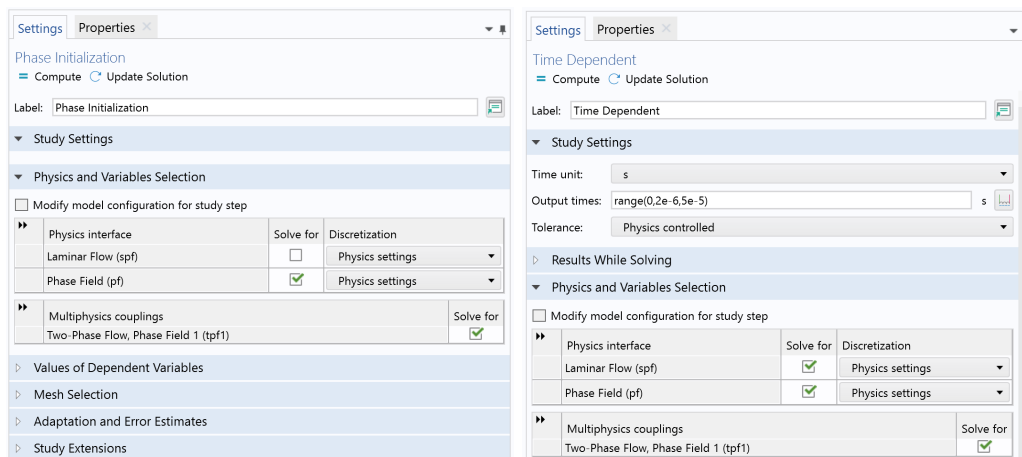


Figure 4.7: Settings for two-step study used to solve the coupled problem.

By means of performing a Parametric sweep for the length of the filament ( $L$ ), it can be proved that in fact there is a critical aspect ratio  $\lambda_s$  below which the filament remains stable and above which the filament thinning process is triggered by capillary forces (Figure 4.8), as discussed before in Section 3.1. This model may also allow to performing different numerical analysis regarding the importance of other parameters in the filament thinning process, such as the surface tension for instance (Figure 4.9), where it can be observed that the larger values of surface tension, the faster the filament breaks up. It may also allows for determining the time evolution of the minimum diameter with time, as it is typically represented the results obtained by means of the CaBER experiments.

To sum up this section, it can be said that the *CaBEERTwoPhaseFlow.mph* model was successfully implemented and it sets the basis for the construction of the *CaBEER.mph* model.

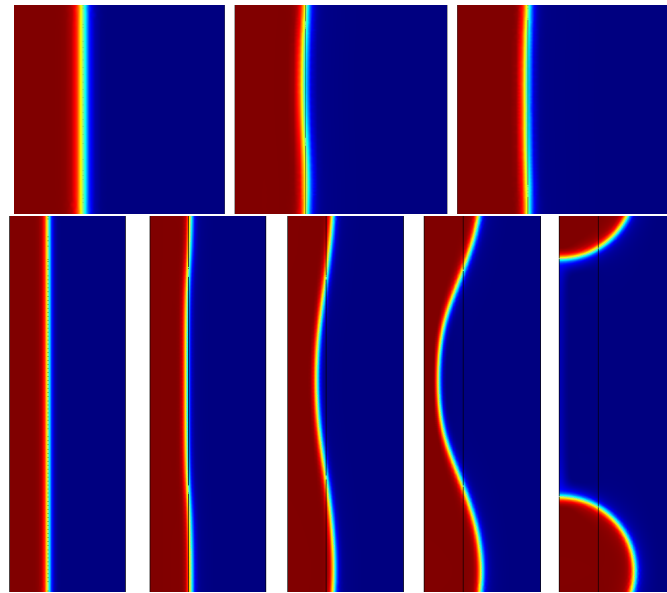


Figure 4.8: Time evolution of the filament silhouette for the same fluid with the same conditions, except for the aspect ratio:  $\Lambda_1 = 1.5$  for 1 ms and no breakup (top row) and  $\Lambda_2 = 5$  for 0.14 ms (bottom row).

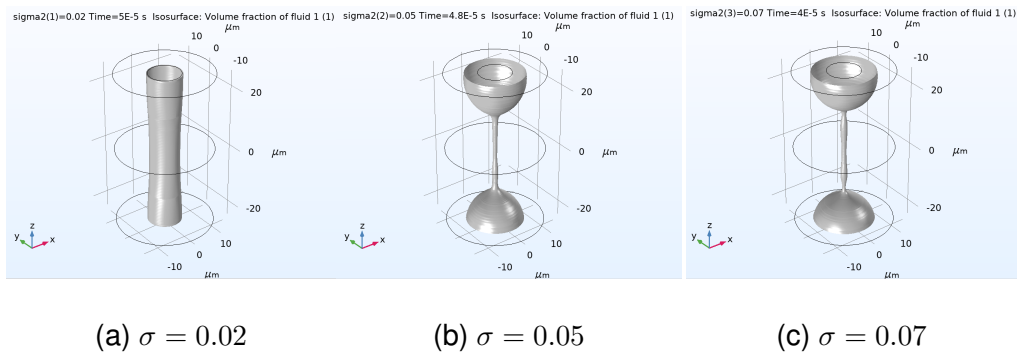


Figure 4.9: Last filament silhouette before breakup for the same fluid with the same conditions, except for the surface tension coefficient. In the case of the  $\sigma = 0.02$  the filament was stable.



## 4.2 Particle Tracing for Fluid Flow

This model is contained in the file *ParticleTracing.mph* (Figure 4.10).

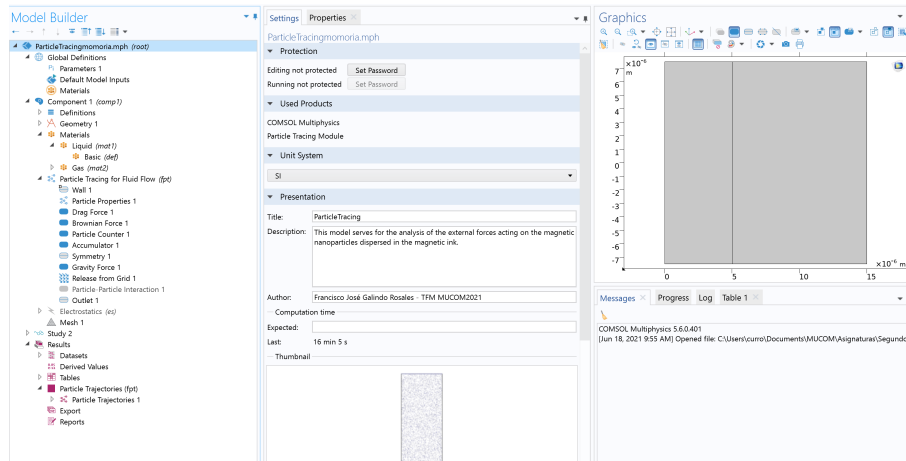


Figure 4.10: Printscreen showing the general view of the Particle Tracing model.

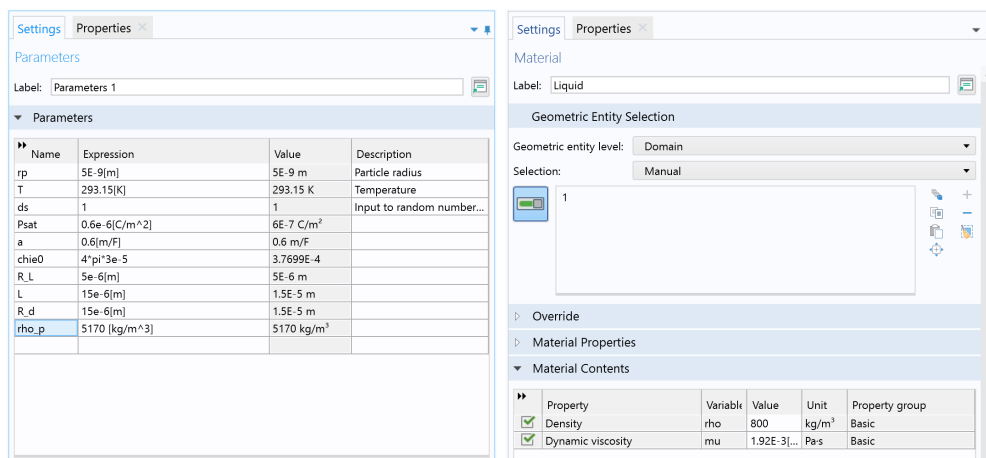


Figure 4.11: Definition of geometric parameters and particle properties required for the Particle Tracing model (left), as well as the properties of the liquid carrying the particles (right).

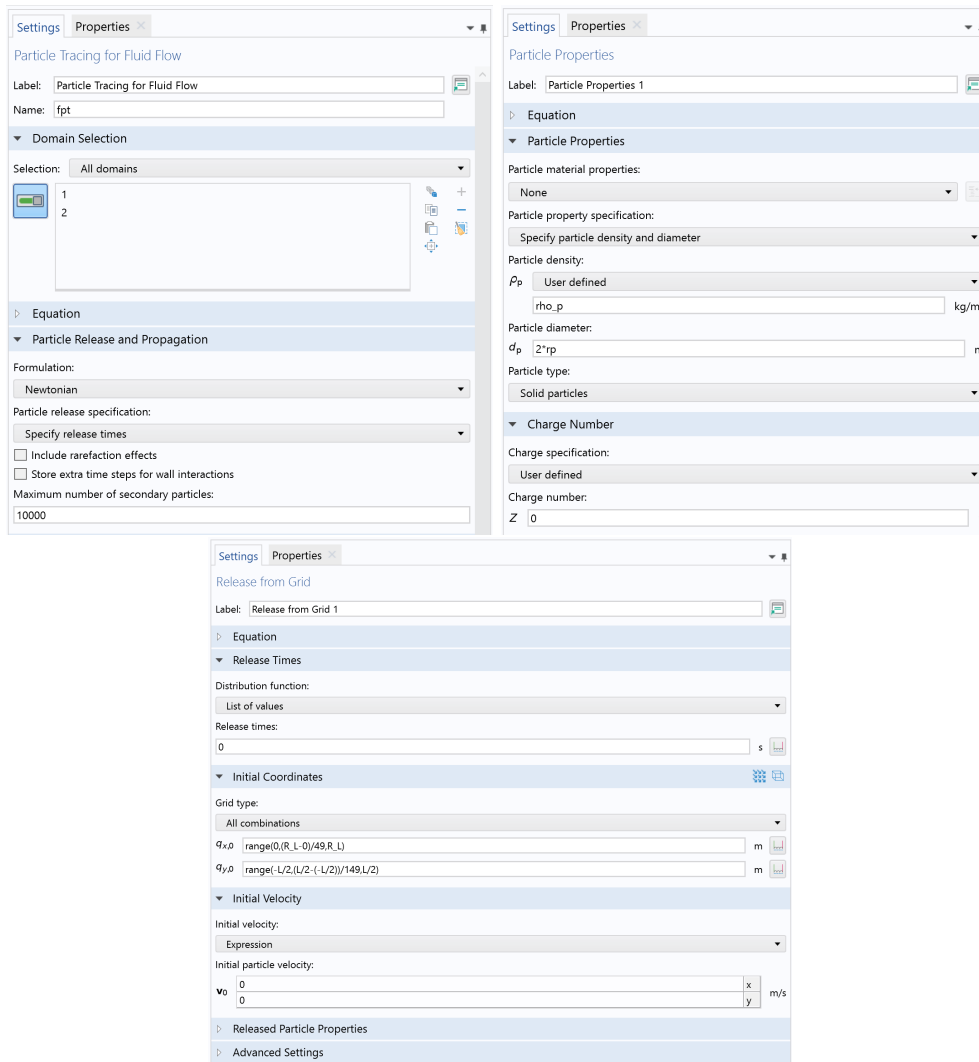


Figure 4.12: Settings for the Particle Tracing for Fluid Flow (top-left), particle properties (top-right) and the release of the particles (bottom).

The geometric parameters referring to the fluid domain are the same as in the *CaBEERTwoPhaseFlow.mph* model. Additionally, the particle size ( $R_p$ ) was added, as well as other intrinsic parameters regarding the polarization (Figure 4.11). Again, the fluid domains are assigned with two materials, which viscosity and density are user-defined as in the previous model. Then, the *Particle Tracing for Fluid*

*Flow* interface is configured for Newtonian formulation in the domain of the liquid sample; additionally, the particle properties are defined, as well as how they are released into the system, i.e. homogeneously dispersed and with no velocity (Figure 4.12). Finally, the boundary conditions are set, maintaining the axis of symmetry, being the top and bottom contours set as outlets through which the particles disappear, and the interphase with the gas a wall where the particles can bounce.

### 4.2.1 External forces

The external forces acting on the particles are the Brownian force, the gravitational force and the drag force, as mentioned above and depicted in Figure 3.3. Consequently, these forces have been introduced into the model (Figure 4.13). As the particle size has been parametrized, it is possible to perform an analysis and determine upon which particle size sedimentation is an issue in less than a millisecond, for instance (Figure 4.14).

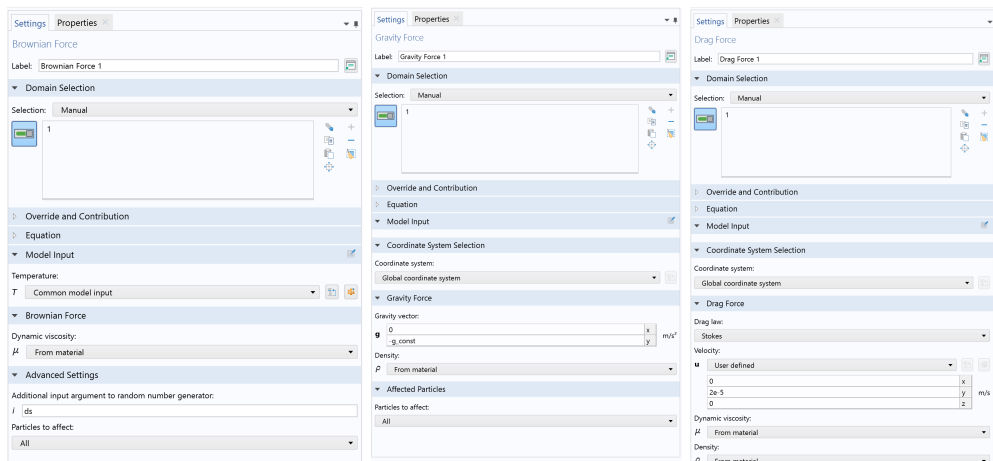


Figure 4.13: Settings for the Particle Tracing for Fluid Flow (left), particle properties (middle) and the release of the particles (right).

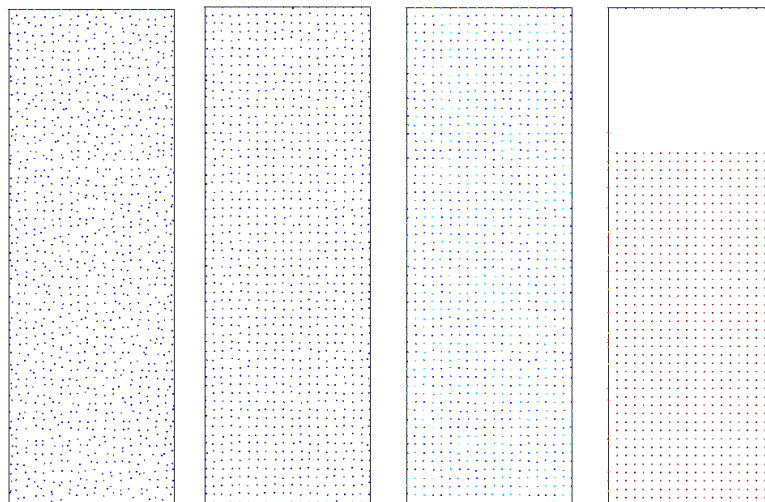


Figure 4.14: Particle trajectories for different particle sizes after 1 ms after having been released:  $r_p = \{100 \text{ nm}, 500 \text{ nm}, 1 \mu\text{m}, 500 \mu\text{m}\}$  (from left to right).

### 4.2.2 Inter-particle force

In order to set the inter-particle force due to the polarization of the magnetic nanoparticles, it is necessary to impose a voltage difference, so that the particle can get polarized. Then the *Electrostatic* interface is added to the model, the top contour of the liquid domain is set to a voltage  $V_0$  and the bottom one to the ground, and the liquid sample is defined as a Ferroelectric material that follows the Langevin Function for its polarization (Figure 4.15). It is just left the definition of the force as a function of the polarization and the relative position between the particles (Equation 3.17). Unfortunately the command to extract that parameter was not found and the force could not be defined properly.

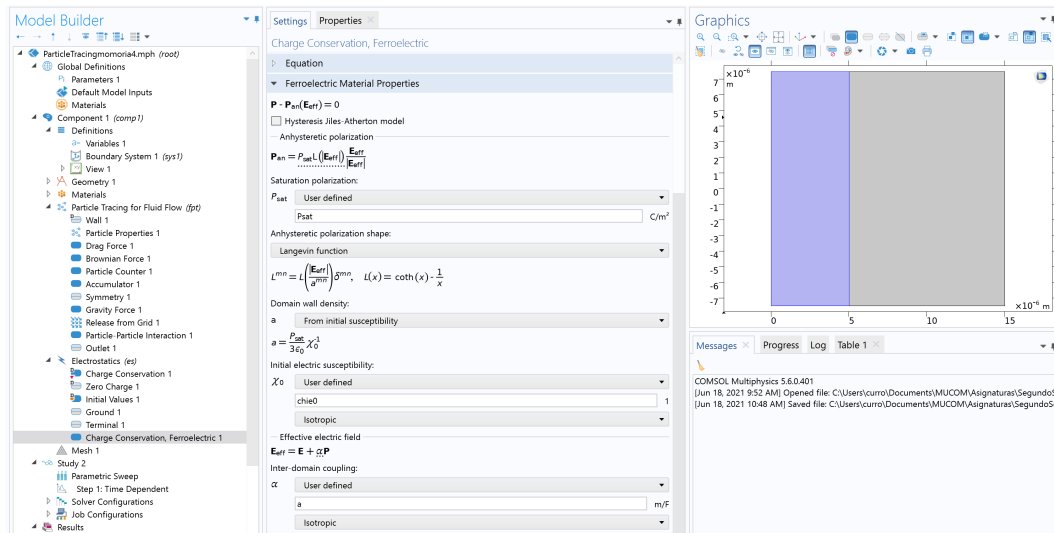


Figure 4.15: The electrostatic interface is added to the model. The liquid domain is set as a Ferroelectric material following the Langevin Function for its polarization.

A new study is defined, wall, consisting of two steps: first, the electric field is determined in stationary; then, the particle tracing is solved out (Figure 4.16)

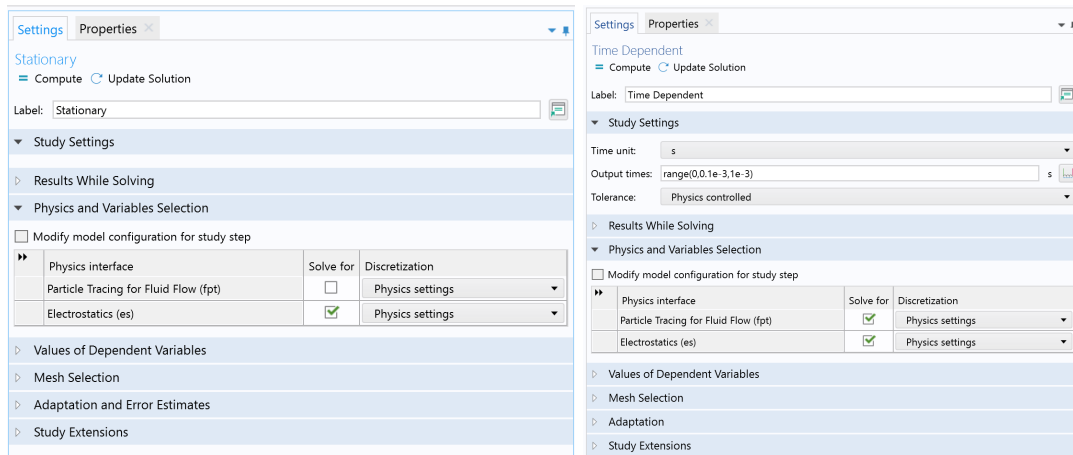


Figure 4.16: Settings for the two-step study in the case of considering the inter-particle force due to polarization.

The solution did not converged and the problem remained unsolved yet (Figure 4.17).

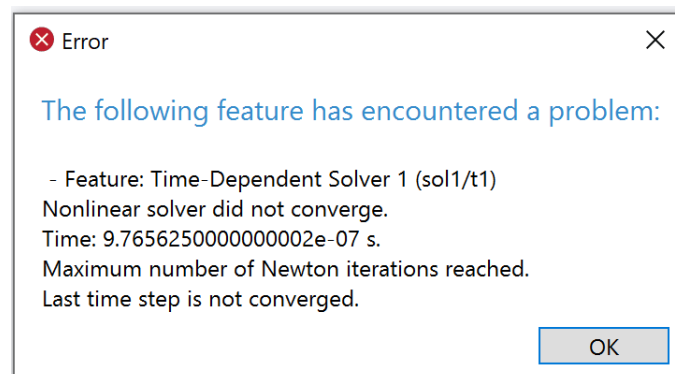


Figure 4.17: Error message when considering the contribution of the polarization forces.

## 4.3 CaBEER model

The two models developed in Sections 4.1 and 4.2 are now combined into *CaBEER.mph* model (Figure 4.18). The only difference with the model of the particle tracing is the definition of the Drag Force; in this case, the velocity field has to be taking from the laminar flow interface (Figure 4.20). Then a new step in the study is added, to solve the position with time of the magnetic nanoparticles.

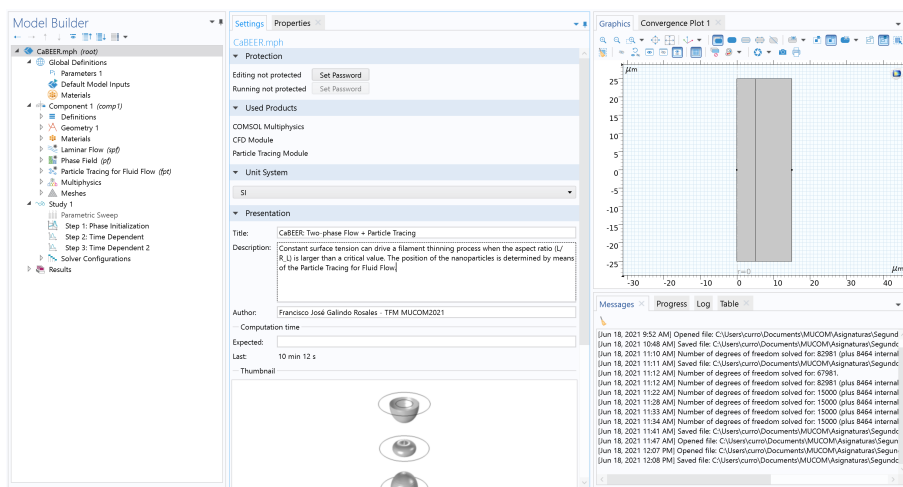


Figure 4.18: Printscreen showing the general view of the CaBEER model.

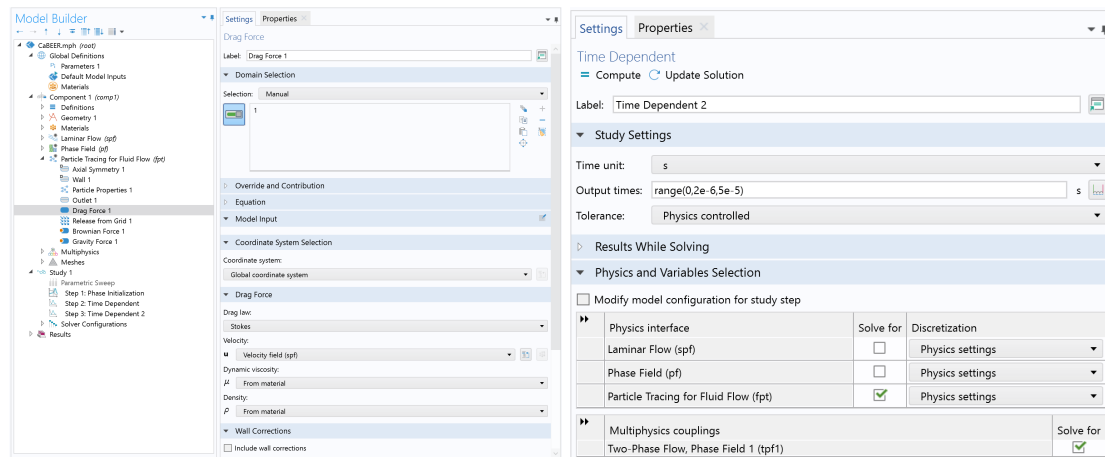


Figure 4.19: Settings for the drag force applied to the particles when coupled with the fluid flow in the liquid sample (left). Settings for the third step in the study, where the Particle Tracing for fluid flow is solved with time after the fluid flow and the interface have been solved first.

Due to the difficulty in getting a converged solution for the case in which the particles are polarized (Section 4.2.2), this inter-particle force have not considered in the current version of the CaBEER model. As a consequence, at the moment, this model is unable of providing meaningful information regarding the influence of the electric field on the capillary thinning process of magnetic inks, as it was aimed at. Still, this model remain useful for the numerical analysis of the different parameters relevant for the formulation of these inks, which is of paramount importance when using this inks with printing process like inkjet printing.



## 4.4 CaBEER-APP

The CaBEER-APP can be run from the file *CaBEERapp.mph*. This application allows the user not familiarized with Comsol Multiphysics to performing numerical simulations of the CaBEER model. The user can design the fluid domain, the fluid properties, consider or not Marangoni Effects, perform parametric sweep análisis, etc. (Figure 4.20).

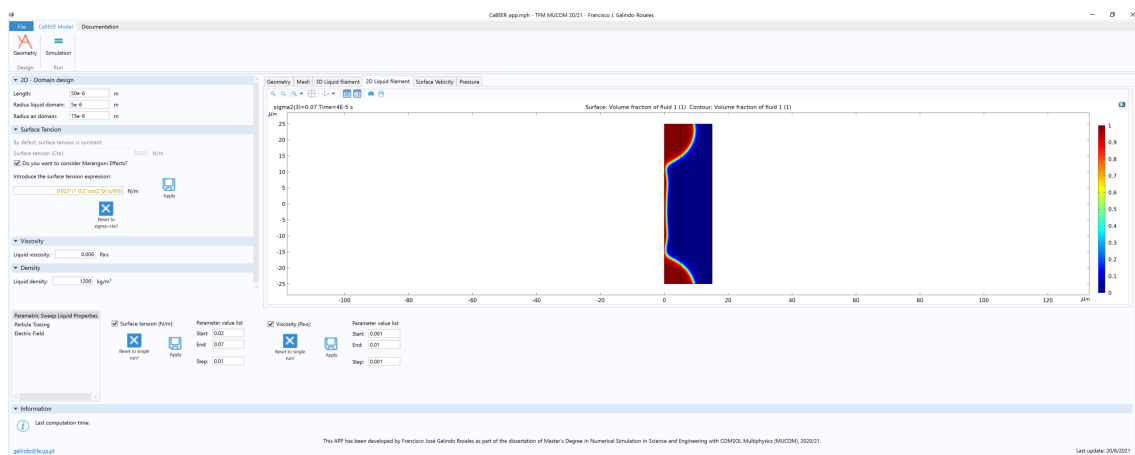


Figure 4.20: Printscren of the CaBEER-APP.



# Chapter 5

## Final remarks and future works

This work aimed at providing a model in COMSOL able to simulate the filament thinning process of functional inks under the presence of an external electric field. The physics of the problem have been rigorously defined and different physics interfaces from COMSOL have been identified as necessary to tackle this problem, namely the *Laminar Flow* and *Phase Field*, both coupled by means of the Multiphysics interface *Two-Phase Flow, Phase Field* to predict the filament thinning process. The magnetic nanoparticles dispersed in the functional ink was modelled by means of the *Particle Tracing for Fluid Flow*, which allows for accounting with the three external forces acting on the nanoparticles (Brownian, drag and gravitational forces) and the inter-particle force due to their polarization under the presence of an external field. Then, the *Electrostatic* module was also set in place. The force due to the polarization could not be properly defined because the dipolar moment was not found; additionally, the model did not converge either. For that reason *CaBEER.mph* model does not consider yet the influence of the electric field in the particles; consequently, the particles cannot form aggregates

and modify the capillary thinning process of the ink.

Then, analysing the stability of a slender, axisymmetric jet under the presence of an external electric field is not yet possible with this model. Nevertheless, it is yet very useful as it allows for analysing how the different parameters in the formulation of the magnetic ink affect the capillary thinning process, which is of paramount importance for non-electric printing techniques, such as the inkjet printing technique.

In the coming future, all efforts will be dedicated to improve this work and introduce in the *CaBEER.mph* model the inter-particle force due to the polarization of the nanoparticles. Once this improved version of the model were available, numerical experiments will be produced so that they could be compared/validated with experimental data.

# Bibliography

- [1] Zhouping Yin, YongAn Huang, Yongqing Duan, and Haitao Zhang. *Introduction of Electrohydrodynamic Printing*, pages 1–29. Springer Singapore, Singapore, 2018.
- [2] W.M. Winslow. Method and Means for Translating Electrical Impulses Into Mechanical Force. US Patent 2,417,850, 25 March, 1947.
- [3] Weijia Wen, Xianxiang Huang, and Ping Sheng. Electrorheological fluids: structures and mechanisms. *Soft Matter*, 4:200–210, 2008.
- [4] J. Hermenegildo García-Ortiz, Samir H. Sadek, and Francisco J. Galindo-Rosales. Influence of the polarity of the electric field on electrorheometry. *Applied Sciences*, 9(24), 2019.
- [5] Gareth H. Mckinley. Visco-elasto-capillary thinning and break-up of complex fluids. *ANNUAL RHEOLOGY REVIEWS*, pages 1–49, 2005.
- [6] J.H. García-Ortiz and F.J. Galindo-Rosales. Capillary breakup extensional electrorheology of ferrofluids for electrohydrodynamics applications. AuxDefense 2020 – 2nd World Conference on Advanced Materials for Defense, 6-8 July, 2020.

- [7] Lev A. Slobozhanin and José M. Perales. Stability of liquid bridges between equal disks in an axial gravity field. *Physics of Fluids A: Fluid Dynamics*, 5(6):1305–1314, 1993.
- [8] A.E. Ostfeld, I. Deckman, A.M. Gaikwad, C.M. Lochner, and A.C. Arias. Screen printed passive components for flexible power electronics. *Scientific Reports*, 5(1):15959, 2008.
- [9] Jialiang Cen, Rungrot Kitsomboonloha, and Vivek Subramanian. Cell filling in gravure printing for printed electronics. *Langmuir*, 30(45):13716–13726, 2014.
- [10] M. Berggren, D. Nilsson, and N. D. Robinson. Organic materials for printed electronics. *Langmuir*, 6(1):3–5, 2007.
- [11] Peter Mack Grubb, Harish Subbaraman, Saungeun Park, Deji Akinwande, and Ray T. Chen. Inkjet printing of high performance transistors with micron order chemically set gaps. *Scientific Reports*, 7(1):1202, 2017.
- [12] Ethan B. Secor. Principles of aerosol jet printing. *Flexible and Printed Electronics*, 3(3):035002, jul 2018.
- [13] Jang-Ung Park, Matt Hardy, Seong Jun Kang, Kira Barton, Kurt Adair, Deep kishore Mukhopadhyay, Chang Young Lee, Michael S. Strano, Andrew G. Alleyne, John G. Georgiadis, Placid M. Ferreira, and John A. Rogers. High-resolution electrohydrodynamic jet printing. *Nature Materials*, 6(10):782–789, jul 2007.
- [14] Changsheng Wu, Halil Tetik, Jia Cheng, Wenbo Ding, Hengyu Guo, Xingtian Tao, Nanjia Zhou, Yunlong Zi, Zhiyi Wu, Huixuan Wu, Dong Lin, and Zhong Lin Wang. Electrohydrodynamic jet printing driven by a triboelectric nanogenerator. *Advanced Functional Materials*, 29(22):1901102, 2019.

- [15] John Rogers. E-Jet (Electrohydrodynamic Jet) Printing. [http://nano-cemms.illinois.edu/media/uploads/content/102/files/e\\_jet.20110826153526.pdf](http://nano-cemms.illinois.edu/media/uploads/content/102/files/e_jet.20110826153526.pdf), accessed in 1 April, 2021.
- [16] Denis S. Kolchanov, Vladislav Slabov, Kirill Keller, Ekaterina Sergeeva, Mikhail V. Zhukov, Andrey S. Drozdov, and Alexandr V. Vinogradov. Sol-gel magnetite inks for inkjet printing. *J. Mater. Chem. C*, 7:6426–6432, 2019.
- [17] Klaas Nijenhuis, Gareth McKinley, Stephen Spiegelberg, Howard Barnes, Nuri Aksel, Lutz Heymann, and Jeffrey Odell. *Non-Newtonian Flows*, pages 619–743. Springer Berlin Heidelberg, Berlin, Heidelberg, 2007.
- [18] Gareth H. McKinley and Tamarapu Sridhar. Filament-stretching rheometry of complex fluids. *Annual Review of Fluid Mechanics*, 34(1):375–415, 2002.
- [19] Laura Campo-Deaño and Christian Clasen. The slow retraction method (srm) for the determination of ultra-short relaxation times in capillary breakup extensional rheometry experiments. *Journal of Non-Newtonian Fluid Mechanics*, 165(23):1688–1699, 2010.
- [20] Samir H. Sadek, Hossein H. Najafabadi, and Francisco J. Galindo-Rosales. Capillary breakup extensional electrorheometry (cabeer). *Journal of Rheology*, 64(1):43–54, 2020.
- [21] Geoffrey Ingram Taylor and M. D. Van Dyke. Electrically driven jets. *Proceedings of the Royal Society of London. A. Mathematical and Physical Sciences*, 313(1515):453–475, 1969.
- [22] Jang-Ung Park, Sangkyu Lee, Sakulsuk Unarunotai, Yugang Sun, Simon Dunham, Taeseup Song, Placid M. Ferreira, Andrew G. Alleyene, Ungyu

- Paik, and John A. Rogers. Nanoscale, electrified liquid jets for high-resolution printing of charge. *Nano Letters*, 10(2):584–591, 2010. PMID: 20067277.
- [23] K. YamadaNaofumi and E. Watanabe. Oil-based magnetic ink . United States patent application US20190031901A1, 31 January, 2019.
- [24] H Block and J P Kelly. Electro-rheology. *Journal of Physics D: Applied Physics*, 21(12):1661–1677, dec 1988.
- [25] A. Wilmer Duff. The viscosity of polarized dielectrics. *Phys. Rev. (Series I)*, 4:23–38, Jul 1896.
- [26] W. M. Winslow. Induced fibrillation of suspensions. *Journal of Applied Physics*, 20(12):1137–1140, 1949.
- [27] W.M. Winslow. Field Controlled Hydraulic Device. US Patent 2,661,596, 8 December 1953.
- [28] W.M. Winslow. Field Responsive Force Transmitting Compositions. US Patent 3,047,507, 31 July, 1962.
- [29] Youngwook P. Seo and Yongsok Seo. Modeling of electrorheological fluids. In *Reference Module in Materials Science and Materials Engineering*. Elsevier, 2020.
- [30] Francisco J. Galindo-Rosales. Complex fluids in energy dissipating systems. *Applied Sciences*, 6(8), 2016.
- [31] Thomas C. Halsey. Electrorheological fluids. *Science*, 258(5083):761–766, 1992.



- [32] MARK R. JOLLY and J. DAVID CARLSON. 5.27 - composites with field-responsive rheology. In Anthony Kelly and Carl Zweben, editors, *Comprehensive Composite Materials*, pages 575–589. Pergamon, Oxford, 2000.
- [33] Samir H. Sadek, Hossein H. Najafabadi, and Francisco J. Galindo-Rosales. Capillary breakup extensional electrorheometry (cabeer). *Journal of Rheology*, 64(1):43–54, 2020.
- [34] F.J. Galindo-Rosales, S.H. Sadek, H.H. Najafabadi, and L. Campo-Deaño. Extensional electro-rheological adapter. Worldwide patent application WO2020208550A1, 15 October, 2020.
- [35] Manuel Rubio, Emilio J. Vega, Miguel A. Herrada, José M. Montanero, and Francisco J. Galindo-Rosales. Breakup of an electrified viscoelastic liquid bridge. *Phys. Rev. E*, 102:033103, Sep 2020.
- [36] Claire McIlroy and Oliver G. Harlen. Modelling capillary break-up of particulate suspensions. *Physics of Fluids*, 26(3):033101, 2014.
- [37] Jianyi Du, Hiroko Ohtani, Crystal E. Owens, Lenan Zhang, Kevin Ellwood, and Gareth H. McKinley. An improved capillary breakup extensional rheometer to characterize weakly rate-thickening fluids: Applications in synthetic automotive oils. *Journal of Non-Newtonian Fluid Mechanics*, 291:104496, 2021.
- [38] Lucy E. Rodd, Timothy P. Scott, Justin J. Cooper-White, and Gareth H. McKinley. Capillary break-up rheometry of low-viscosity elastic fluids. *Applied Rheology*, 15(1):12–27, 2005.
- [39] Laura Campo-Deaño and Christian Clasen. The slow retraction method (srm) for the determination of ultra-short relaxation times in capillary breakup

- extensional rheometry experiments. *Journal of Non-Newtonian Fluid Mechanics*, 165(23):1688–1699, 2010.
- [40] A. Ieta, C. Wahl, D. Quill, J. Primrose, and J. Moody. Electro spray Patterns of Oil-based Ferrofluids. Proceedings of the 2011 ESA Annual Meeting on Electrostatics. Case Western Reserve University, Cleveland OH., June 14-16, 2011.
- [41] Inc Ferrotec. EMG Series - Oil-based Ferrofluid. Type: EMG 905. <https://ferrofluid.ferrotec.com/products/ferrofluid-emg/oil/emg-905/>, accessed in 12th May, 2021.
- [42] Anna Spanoudaki and Rolf Pelster. Frequency dependence of dielectric anisotropy in ferrofluids. *Journal of Magnetism and Magnetic Materials*, 252:71–73, 2002. Proceedings of the 9th International Conference on Magnetic Fluids.
- [43] Osman A. Basaran and Fred K. Wohlhuter. Effect of nonlinear polarization on shapes and stability of pendant and sessile drops in an electric (magnetic) field. *Journal of Fluid Mechanics*, 244:1–16, 1992.
- [44] Bastian E. Rapp. Chapter 20 - surface tension. In Bastian E. Rapp, editor, *Microfluidics: Modelling, Mechanics and Mathematics*, Micro and Nano Technologies, pages 421–444. Elsevier, Oxford, 2017.
- [45] Jan Mewis and Norman J. Wagner. *Colloidal Suspension Rheology*. Cambridge University Press, 1st edition, 2012.
- [46] Wouter Mathues, Claire McIlroy, Oliver G. Harlen, and Christian Clasen. Capillary breakup of suspensions near pinch-off. *Physics of Fluids*, 27(9):093301, 2015.

- 
- [47] Ed Fontes. Modeling and Simulation of Multiphase Flow in COMSOL. COMSOL Blog: <https://www.comsol.com/blogs/modeling-and-simulation-of-multiphase-flow-in-comsol-part-1/>, Accessed in 14 June, 2021.
- [48] COMSOL. CFD Module User's guide. COMSOL 5.6. Part number: CM021301. <https://doc.comsol.com/5.6/doc/com.comsol.help.cfd/CFDModuleUsersGuide.pdf>, Accessed in 14 June, 2021.
- [49] COMSOL. AC/DC Module User's guide. COMSOL 5.6. Part number: CM020101. <https://doc.comsol.com/5.6/doc/com.comsol.help.acdc/ACDCModuleUsersGuide.pdf>, Accessed in 14 June, 2021.
- [50] K. V. Erin and Yu. I. Dikanskii. Using the electrooptic effect to study charge relaxation in colloidal solutions of magnetite. *Technical Physics Letters*, 35:467–469, 2009.
- [51] COMSOL. Particle Tracing Module User's guide. COMSOL 5.6. Part number: CM022701. <https://doc.comsol.com/5.6/doc/com.comsol.help.particle/ParticleTracingModuleUsersGuide.pdf>, Accessed in 16 June, 2021.



